Effects of Molecular Structure and Packing Order on the Stretchability of Semi-Crystalline Conjugated Poly(tetrathienoacene-diketopyrrolopyrrole) Polymers

Chien Lu, Wen-Ya Lee, Xiaodan Gu, Jie Xu, Ho-Hsiu Chou, Hongping Yan, Yu-Cheng Chiu, Mingqian He, James R Matthews, Weijun Niu, Jeffery B.-H. Tok, Michael F. Toney, Wen-Chang Chen and Zhenan Bao*

[*]Chien Lu, Dr. Xiaodan Gu, , Dr. Jie Xu, Dr. Ho-Hsiu Chou, Dr. Yu-Cheng Chiu, Dr. Jeffery B.-H. Tok, Prof. Zhenan. Bao
Department of Chemical Engineering, Stanford University
Stanford, California 94305, United States
E-mail: zbao@stanford.edu

Prof. W.-Y. Lee
Department of Chemical Engineering and Biotechnology,
National Taipei University of Technology, Taipei 106, Taiwan,

Dr. Hongping Yan and Dr. Michael F. Toney
Stanford Synchrotron Radiation Lightsource, SLAC National Accelerator Laboratory, Menlo Park, California 94025, United States

Dr. Mingqian. He, Dr. James R Matthews, Dr. Weijun Niu
Corning Incorporated, One River Front Plaza,
Corning, New York 14831, United States

Chien Lu, Prof. W.-C. Chen
Department of Chemical Engineering, National Taiwan University
Taipei, 10617 Taiwan

Abstract

The design of polymer semiconductors possessing high charge transport performance, coupled with good ductility, remains a challenge. Understanding the distribution and behavior of both crystalline domains and amorphous regions in conjugated polymer films, upon an applied stress, should provide general guiding principles to design stretchable organic semiconductors. Structure-property relationships (especially in both side chain and backbone engineering) were investigated for a series of poly(tetrathienoacene-diketopyrrolopyrrole) polymers. We observed that the fused thiophene diketopyrrolopyrrole-based polymer, when incorporated with branched side chains and an additional thiophene spacer in the backbone, exhibited improved mechanical endurance and, in addition, did not show crack propagation until 40% strain. Furthermore, this polymer exhibited a hole mobility of 0.1 $cm^2V^{-1}s^{-1}$ even at 100% strain or after recovered from strain, which reveals prominent continuity and viscoelasticity of the polymer thin film. We also observed that the molecular packing orientations (either edge-on or face-on) significantly affect the mechanical compliance of the polymer films. The improved stretchability of the polymers was attributed to both the presence of soft amorphous regions and the intrinsic packing arrangement of its crystalline domains.

Introduction

Recently, polymer-based electronics have shown significant progress in terms of flexibility as well as bendability.[1,2] However, there are only a few reports of stretchable polymer electronics.[3,4] Due to high crystallinity and rigid polymer backbone, semiconducting polymers typically exhibit high tensile moduli and a high degree of brittleness, leading to rapid degradation of electrical properties during stretching.[5-7] In this regard, maintaining both the charge transport properties and ductility is a challenge for developing polymers for novel stretchable electronic applications.[8,9]

π-conjugated polymers, such as polythiophene or donor-acceptor polymers, show high backbone coplanarity and crystalline packing due to their rigid polymer chains and strong π-π interaction.[10] Nevertheless, the presence of large fractions of interconnected crystalline domains in the solid state, a lack of significant chain folding and/or coiling, and high glass transition temperatures contribute to the high tensile moduli of polymer films and make these films too rigid to release the applied stress. In contrast, for polymer thin films containing properly engineered crystalline and amorphous regions, such as polyurethane and elastic polypropylene, the applied stress is preferentially dissipated in the relatively softer amorphous regions. Similar to other reported semi-crystalline polymers, the tensile properties are influenced by the detailed morphology of both the amorphous and crystalline domains. The presence of

a modest fraction of crystalline domains (e.g. 12% for thermoplastic polyurethane and 10% for elastic polypropylene) is able to improve the tensile strength and elasticity of polymer thin films.[11,12] The crystalline packing arrangement and properties of conjugated polymers are both governed by the structure of the side chains and polymer backbones, which will affect the resulting thin film morphology of crystalline and amorphous regions. These features of semi-crystalline conjugated polymers suggest, not surprisingly, that the side chain and backbone engineering influences the polymer thin film mechanical compliance.

A limited number of studies on the mechanical properties of conjugated polymer have been published recently.[13-21] Polymers with branched alkyl side chains have been reported with lower fracture strain than those with linear alkyl side chains.[13-15] Increasing side chain length was found to lower the tensile moduli and glass transition temperatures to make the target conjugated polymer more 'rubber-like' at ambient temperatures.[16,17] Savagatrup et al. reported on the stretchability of regio-regular poly (3-alkylthiophene) (P3AT) as a function of the length of linear alkyl side chains, observing that the longer alkyl side chains reduced the modulus of the thin film.[5,18] They also found using poly[2,5-bis(3-alkylthiophen-2-yl)thieno(3,2-b)thiophene] (pBTTT) and regioregular polyquaterthiophene (PQT) that stronger side chain interdigitation density appeared to preserve the lateral ordering structure in

three-dimensional packing, however, the packing interaction of pBTTT may lead to a significantly higher brittleness than P3HT.[7,19,20] Furthermore, Jin et al. found that long branched alkyl side chains not only reduced the order of alkyl chain packing in the crystalline domains, but they also 'softened' the disordered amorphous thin film.[21]

The understanding of the relationship between molecular packing structure and mechanical compliance of polymer thin film remains limited.[22,23] It has been shown that tailoring the backbone planarity enables either preferential backbone edge-on or face-on packing structures.[24] The backbone planarity is mainly affected by the chemical structures of the adjacent monomer units.[25] Conjugated polymers with fused aromatic rings and donor-acceptor structures tend to favor strong π-stacked structure leading to relatively high crystallinity and good charge carrier mobility.[26,27] In addition, strategic placement of side-chains may reduce torsion and steric effects of side-chains, thus improving the planarity and backbone conjugation to promote a more ordered solid-state packing structure.[28,29]

Based on the above considerations, we have prepared conjugated polymers with different alkyl side chains and backbones (structures shown in Figure 1). Poly(tetrathienoacene-diketopyrrolopyrrole) (PTDPPTFT4, P1) with linear side chains was previously reported to exhibit planar backbone geometry and crystalline packing.[27,30] The use of the branched alkyl side chains in the DPP moiety (P2) is

expected to soften the amorphous region of polymer thin film. In addition to the change to branched side chains, additional thiophene spacers were also inserted in the backbone (P3). The thiophene spacers allowed us to tune the planarity of the polymer backbone, such that we can better elucidate how the packing arrangements may affect mechanical properties. To verify our aim in comparing the mechanical property and crystalline packing structure, we performed mechanical, morphological, and electrical characterizations under different stretching conditions. These results were found to be primarily dominated by factors such as the effect of alkyl side chains on their amorphous region, the film continuity with applied strain, and the polymer crystallite orientation. Our results and understanding will assist the molecular design of future conjugated polymers with both high electrical performance and stretchability.

Result and discussion

Thermal and mechanical dynamic behaviors of bulk polymers

The molecular weight of all polymers studied are similar as measured by Gel Permeation Chromatography (GPC) at moderate temperatures (Table 1). The studied polymers displayed different thermal and mechanical properties in bulk solid state. The powder of P1 appears relatively brittle, while P2 and P3 are soft and slightly sticky at ambient temperature. The bulk polymers were evaluated by differential

scanning calorimetry (DSC) by continuous heating and cooling as shown in Figure 2a. P1 exhibited one endothermic transition (50 °C) upon heating and one exothermic transition (50 °C) during the cooling processes. This is attributed to the melting (disordering) and crystallization (ordering) processes associated with the linear alkyl side chains.[27] On the other hand, there is no melting or crystalline thermal transition that could be observed for P2 and P3 in the temperature range from 0^{o}C to 300^{o}C. This suggests that the semiconducting polymers with linear alkyl side chains can partially crystallize while the semiconducting polymers with branched side chains are primarily disordered.

The glass transition temperatures of the branched alkyl side chains containing polymers P2 and P3 were readily observable in DSC thermograms. To investigate the glass transitions of these polymers, films of each conjugated polymer (200-250 nm thick) on polyimide substrates (600 nm thick) were studied using Dynamic Mechanical Thermal Analysis (DMA) as shown in Figure 2b. This method was previously reported by Akabori et al to measure the thermal dynamic viscoelastic behavior of ultrathin polystyrene films.[31] Since the polyimide substrate has no observable glass transition temperature within the measurement temperature range and gives a relatively monotonic curve, the transition peak observed at 4.3 °C is attributed to P1's glass transition. Using the same characterization method, the glass

transition temperatures of P2 and P3 were determined to be both around -48 °C, which is much lower than that of P1. The significant difference in glass transition temperature (T_g) between the polymers is also affected by the different side chain interchain distance and bulkiness. The T_g's of P2 and P3 are much lower than ambient temperature, suggesting that P2 and P3 have domains that may be more rubber-like than P1 at room temperature. The higher T_g and T_m of P1 is consistent with its more brittle property in the bulk. As a result, introducing branched alkyl side chain could significantly affect the viscoelastic behaviors of the bulk phase of the conjugated polymers.

Elastic moduli of polymer thin film

To investigate the mechanical properties of our three conjugated polymers, we measured the elastic moduli using a buckling metrology method,[32] which uses the modulus mismatch between a pre-strained polydimethylsilox-ane (PDMS) substrate at 4% strain and a polymeric thin film of interest with different thicknesses between 30-400 nm. The polymeric thin films were transferred from a host octadecyltrichlorosilane (OTS)-treated substrate to a pre-strained PDMS substrate followed by release of the straining PDMS substrate. The transferred film was compressed (due to the modulus mismatch) which led to the formation of periodic

buckles. The optical images of thin films on pre-strained PDMS substrates are shown in Figures 3 and S1. The buckling wavelengths (λ_b) as a function of film thickness (d_f) was plotted in Figure 3c. To calculate the elastic moduli of the thin films, we use the slope derived from the linear fit (λ_b/d_f,) via the following Equation 1:

$$E_f = 3E_s\left(\frac{1-\nu_f}{1-\nu_s}\right)\left(\frac{\lambda_b}{2\pi d_f}\right)^3 \qquad \text{(Eqn 1)}$$

where v_f and v_s are the Poisson ratios of the conjugated polymer films (~0.35) and the PDMS (~0.5) substrate, respectively. The tensile moduli of P1, P2, and P3 were determined to be 4.44, 2.39, and 0.82 GPa, respectively. We observed that the P1 thin film showed brittle qualities and it started to form cracks even at 4% pre-strain (optical images in Figure S1). Thus, a large wave amplitude was observed, which might give rise to an overestimation of its relatively high tensile modulus value relative to other reported conjugated polymers.[7] P2, with branched alkyl side chains, showed evidence of being a softer thin film than P1. This may be attributed to its longer inter-chain distance and lower crystallinity (vide infra). Interestingly, the tensile modulus of P3 was much smaller than P1 or P2, close to the values of diketopyrrolopyrrole- thieno[3,2-b]thiophene copolymer (DPPT-TT) reported previously by our group,[6] indicating that incorporating the tetrathienoacene moiety in the P3 backbone did not affect the thin film state modulus relative to DPPT-TT. However, neither the glass transition nor the viscoelastic behavior of the bulk

materials of P2 and P3 correlate with the difference in their tensile moduli. Since tuning the polymer structure can significantly improve its mechanical compliance, we proceeded to investigate the influence of the stretching behavior on the morphologies and electrical properties of their thin films.

Morphology and electrical performances of polymer thin films

The microstructures of the polymer thin films have been shown to impact both mechanical and electrical properties.[2,3] To investigate the fracture strain of our polymers, both optical microscopy and tapping mode atomic force microscopy (AFM) were performed under different strains.

The optical micrographs in both bright and dark field are shown in Figures 4, S2 and S3. The dark-field images are used to distinguish between cracks and buckles. Without stretching, the transferred thin films of the three polymers all showed smooth and flat surfaces. After stretching, we observed the formation of both cracks and buckles. For P1, at 10% strain, large buckles perpendicular to the stretching direction were formed, along with some cracks longer than 10 μm. When further stretched at 20-50% strain, the P1 film was broken by many shorter cracks. At 50-100% strain, the sizes of the cracks formed became smaller, but the crack and buckling densities became higher. This indicates that the P1 film is highly rigid and tends to form severe

cracks to relieve the applied stress. For P2, the crack-onset strain is near 20%. However, with stretching to 100%, the crack density increases, but the crack size only became slightly larger. Additionally, compression stress was formed in the perpendicular direction during the stretching process, which leads to the formation of buckles. P2 films showed similar buckling density to P1 films (albeit much smaller buckles), indicating that P2 could tolerate higher compression stress than P1. When compared to both P1 and P2, P3 exhibited a smoother surface, even at 30% applied strain. The crack-onset strain of P3 was 40 %. The cracks became larger and at a higher density when subjected to higher strains. However, the thin film of P3 showed a lower crack density and smaller-sized cracks when subjected to a larger strain, as compared to the P1 and P2 films. After being released from strains at both 50% and 100% (which are higher than the crack-onset points of the polymers), wrinkles were also observed on the thin film surface.

The polymer film surface morphologies were also further investigated with AFM (1 μm × 1 μm), as shown in Figures 5 and S4. Generally, the three films displayed worm-like or nano-fibrillar textures before stretching. Of particular interest, the texture of P3 maintained a similar continuous nano-fiber morphology even when subjected to 50% strain. This indicates that the nano-fibrils can remain continuous and entangled under mechanical strain.[33] Furthermore, the entanglement and interlacing of

nano-fibers may provide both stronger interactions and/or attractions to impart better ductility characteristics. These nanofibrils were disordered and separated at 100% strain due to the formation of cracks. On the other hand, the phase images acquired for P1 and P2 films were observed to change significantly when strain was applied. The original textures were changed entirely and the nanofibril structures became less clear. Moreover, both cracks and buckles were still observed even at 1 μm×1 μm scale, indicating that the crack density in the P1 and P2 films was faster to develop than the crack density in P3 film. The height and phase images at larger scale (5 μm × 5 μm) for P2 and P3 at 50% strain are also provided in Figure S5, showing that the cracks on P2 film were as deep as the film thickness (~40 nm). However, the depth of the cracks in the P3 films were much shallower than the film thickness, suggesting that the film continuity could be maintained when stretched.

The electrical characteristics were measured by transferring polymeric thin films onto the silicon oxide gate dielectric of a bottom gate, with subsequent deposition of top contact electrodes to form FETs with channel lengths (L) of 50 μm. We note that the size of a single device is much larger than the crack size in our polymer thin films. Typical transfer and output curves of these devices are shown in Figure S6. Both the p-channel mobilities and drain current values shown in Figure 6 are for films subjected to strain from 0% to 100% and then the strain released from

50% and 100%, in both parallel and perpendicular stretching directions. The detailed on/off ratio and threshold voltage values at each applied strain and directions are summarized in Figure S7. The charge transport mobility of P3HT is reported to increase along the direction of strain, but decreases along the perpendicular direction.[2,22,23] We again note that our DPP-based polymers not only exhibited higher charge transport performance, but also showed different behaviors upon stretching likely due to their different crystalline structures and orientations. Compared to the performance of pristine FETs on OTS-treated substrates, these thin films did not show significant degradation of electrical properties after being transferred to another substrate. Furthermore, the trend of mobilities and drain current on straining are similar during stretching and releasing. Moreover, the off current and gate leakage current remained at the same level in the range from 0% to 100% of applied strain. These results indicated the polymeric thin films were not damaged during the film transferring process.

Our three polymers all exhibited different trends in mobility when stretched. The mobility of P1 parallel to strain direction significantly decreased as the applied strain increased, dropping two orders of magnitude by 100% strain. However, the mobility perpendicular to the strain direction decreased just less than one order of magnitude at 50% strain, and it remained at the same value in the range of 50% to 100% strain. The

films released from 50% strain showed higher mobility than those released from 100% strain. P1 thin films are not able to recover their initial electrical performance after being subjected to high strain of 100%. For P2, consistent with the trend we have previously observed in film morphology (Figure 4), the softness in the bulk phase can slightly delay the crack-onset point. Devices made from films of P2 exhibited relatively lower mobilities in unstrained thin films than P1, but the mobility of the P2 device can be maintained at up to 50% strain. The recoverability of P2 and P3 were better than P1, which we attribute to their intrinsic softness and viscoelasticity contributed by alkyl branched side chains. P3 exhibited charge mobility as high as P1 before the films were stretched, and more importantly, the mobility of P3 can be maintained at the same order of magnitude even when stretched to 100%. From 0% to 50%, the parallel mobility increased slightly, but began to decay beyond 80% strain. Based on the above observed morphological and electrical characterizations, we conclude that the film continuity of strained polymer films, which can be enhanced by incorporating with branched alkyl side chains in polymers to lower their T_g and tensile moduli in thin film state, give rise to different charge transport properties with strained and released from strain. However, there is still a difference between P2 and P3, which show similar thermal properties but different fracture behavior. This indicates that not only the thin film softness but other factors influence the

stretchability of polymers.

The packing order and their behavior with applied strain

The molecular packing of the polymers P1, P2, and P3 in the thin film state was investigated using Grazing-Incidence X-ray Diffraction (GIXD) to determine the relationship between crystalline packing and chemical structures and to further understand the impact of applied axial strain on the molecular ordering of the films.

The polymer films were prepared by transferring either the stretched or unstrained films from a PDMS substrate to a UV-ozone treated silicon wafer. Both the thin films, with or without strain, were measured using X-ray beam parallel to the strain direction and are shown in Figure S8. For the film with stretching, Figure 8a shows the one-dimensional (1D) profiles of P1 and P3 for near out-of-plane scattering and the 1D profile of P2 for both in-plane (q_{xy}) and near out-of-plane (q_z); these are plotted as intensity (in arbitrary units) *vs* the scattering vector (q ($Å^{-1}$)). The presence of lamella peaks in both q_{xy} and q_z directions shows the P2 crystallites are aligned both face-on and edge-on. For the transferred polymer thin films without applied strain, both P1 and P3 displayed well-defined (h00) peaks along the out-of-plane q_z axis corresponding to an ordered lamellar structure. The (100) peaks of P1 and P3 have shoulder peaks which are a result of artifacts due to the grazing incidence X-ray

geometry for incidence angles close to critical angle of polymers (0.12°).[34] Briefly, the X-rays reflected from the silicon substrate generate another set of diffraction peaks. Note that using a 0.2° grazing incidence angle can eliminate these artifacts, although at a significant sacrifice in the peak intensity. The example of (p-DTS(FBTTh$_2$)$_2$, 7,7′-[4,4-Bis(2-ethylhexyl)-4H-silolo[3,2-b:4,5-b′]dithiophene-2,6-diyl]bis[6-fluoro-4-(5′-hexyl-[2,2′-bithiophen]-5-yl)benzo[c][1,2,5]thiadiazole]) with different incident angles was shown in Figure S9 to illustrate the reflectance effect.

The main (100) peaks appeared at q_z = 0.236 Å^{-1} and 0.267 Å^{-1} for P1 and P3, respectively. Moreover, in Figure S8a, P1 showed two well-defined in-plane diffraction peaks at 1.48 Å^{-1} and 1.74 Å^{-1}, which are attributed to the scattering of the alkyl side-chain packing and backbone π–π stacking, respectively.[30] Similarly, the in-plane diffraction for P3 at 1.68 Å^{-1} is produced by the in-plane π–π stacking packing. For P1 and P3, the π–π stacking along the in-plane direction and strong lamella stacking out-of-plane indicate that the polymers adopt edge-on packing. On the other hand, the polymer thin film of P2 displayed lamellar diffraction peaks in both the q_{xy} and q_z directions (q = 0.241 Å^{-1} in out-of-plane and q = 0.250 Å^{-1} in in-plane, respectively), indicating the presence of a mixture of edge-on and face-on packing. However, the π–π stacking peak is only weakly observed along q_z, which is presumably a result of the hindered packing from the bulky branched alkyl chain size

on DPP. The poorer ordering in P2 can also be inferred from overall lower intensities, the broader peaks and the lack of high-order (h00) peaks. Hence, the more oriented edge-on packing of P1 and P3, and the bimodal lamella orientation of P2 show that the introduction of branched alkyl side chains and thiophene spacers influences both the polymer packing orientation and crystallinity. The d-spacing values of lamellar and π–π stacking peaks were summarized in Table 1.

Different changes in packing structures were also observed when films were stretched. Before we discuss the result from GIXD, ultraviolet–visible (UV–vis) spectrometry equipped with a rotating polarizer was used to characterize the polymer backbone alignment due to strain. The dichroic ratio is defined as $R = A_{\parallel}/A_{\perp}$, where $A_{\parallel}$ is the peak absorbance of the polymer film with polarized light parallel and $A_{\perp}$ is the peak absorbance perpendicular to the stretching direction. The change of $A_{\parallel}$ and $A_{\perp}$ showed similar trend as the polar angle FWHM did during stretching, which are shown below. The alignment of the polymer chains is expected to occur during stretching before cracks start to form and result in an increase of the dichroic ratio value. However, the strain-induced alignment of polymer chains would be interrupted as the cracks formed. After the crack formation and strain release, the aligned and stretched polymer chains recover back abruptly and the dichroic ratio was observed to decrease for P1 and P2, as can be seen in Figure 7. On the other hand, the dichroic

ratio of P3 kept increasing in higher strain levels before 50%, which is close to its crack-onset point. The trend of dichroic ratio with strain in Figure 7 suggests that the alignment of polymer chains occurs before crack formation.

Compared with the alignment of polymer chains with applied strains, the 1D GIXD profiles of each polymer at 0% to 100% strain and recovered from 100% strain are shown in Figures 8b-d and Figure S10, providing the polymer morphology before and after crack-onset points. P1 and P3, consisting of mostly edge-on packing, exhibited similar trend during stretching (i.e. remaining largely edge-on). P3 showed a broader lamellar packing peak in the out-of-plane direction than P1, which may be due to the presence of linear and branched alkyl side chains, and a weaker π-π stacking intensity than P1 in in-plane direction. Interestingly, the d-spacings of lamellar packing for P1 and P3 did not change as the strain increased. For P1, the crack propagation occurred quickly at strain less than 10%. The strain energy was primarily dissipated through crack formation and expansion of cracks after crack onset. Therefore, P1 films after strain relief still maintained similar packing order as initial film. This is consistent with alignment of polymer chains under strain as observed from UV-vis dichroic ratio as a function of strain as discussed later. For P3, the d-spacings are also unchanged by strain. This may be due to the presence of more disordered regions in P3, which allows stress dissipation during strain.[35] Such

disordered regions may be the result of the weaker side-chain inter-digitation of the branched side chains of P3.

The crystalline orientation of polymer films was characterized by the polar angle intensity distribution of diffraction peaks or pole figure.[36] As shown in Figures S11 & S12, the FWHM of the (200) pole figure of our polymers, as calculated from Lorentzian fits, slightly increased up to the crack onset point and recovered back after the strain was released. We also observed that the applied strain disturbed the ordered crystalline domains before forming cracks. Films that were recovered from either 50% or 100% strains showed similar pole figure FWHM values as that of original film at 0% strain, which shows that the orientation of crystallites recovered after strain release. On the other hand, as shown in Figure 8, the diffraction intensities were also observed to increase near the crack-onset point, but began to decrease after the crack-onset point. Before crack propagation, the intensities are somewhat different, which might be due to the deviation from film fabrication. However, a common phenomenon for the polymers is that the diffracted intensity grows to 1.4~2 times larger than the unstretched film. This indicates that, during stretching, the applied strain may enhance the overall crystallinity of thin film due to strain-induced crystallization of amorphous domains into crystalline domains. Similar phenomenon were observed for rubber polymers containing semi-crystalline segments.[37] However,

the changes in crystallite orientation disappeared after cracks formed as the stress was released by cracks. The intensity increase may suggest that stretching of the polymer thin films causes the polymer chains to crystallize which is confirmed by the increased dichroic ratio in UV-vis. Nevertheless, the slightly-increased FWHM before crack propagation might be due to that the rotation or slide-slip of polymer chains which may cause increased disorder in crystalline domains. Interestingly, upon releasing the strain, the X-ray diffraction pattern returned to similar pattern as that of 0% strain, because the strained films were released after crack propagation.

To probe how applied strain affects the packing structures, the 1D profiles of P2 (Figures 8c & 8d) were compared for different strains at both out-of-plane and in-plane directions. The peak information of the polymer films was summarized in Table 1. We found that the lamellar d-spacing in the out-of-plane direction did not change. However, the lamellar d-spacing in the in-plane direction significantly increased from 0 to 20% strain (24.93 Å at 0%, 25.23 Å at 10%, and 26.09 Å at 20%, respectively), and then returned back to 24.83 Å after crack propagation started. The strained P2 films were also measured with X-ray beam perpendicular to the strain direction. The increase of d-spacing in the in-plane direction also occurred and showed similar values, as shown in Figure S12. These results show the d-spacing

values can be recovered after crack formation or releasing the applied strain. On the other hand, the π-π stacking d-spacing of the three polymers did not change before or after crack propagation despite their different packing orientations. Collectively, the above observations suggest that the strain has a great impact on the crystalline ordering and orientation before crack propagation and the ordering can be recovered back after crack propagation.

The schematic packing representations in crystalline domains and the stretching effect on packing behavior of our polymers are illustrated in Figure 9. The dramatic shift in P2's in-plane d-spacing revealed that before the formation of cracks, the crystalline lamella packing distance increased due to the applied strain. However, the d-spacings of all three polymers' out-of-plane diffractions were unchanged. Since the stress was in the plane direction or parallel to the substrate plane, it caused the increase in the d-spacing of lamellar packing in the in-plane direction of the alkyl chains of P2, which we believed results from the applied strain pulling on the lamellar layer separated by side chains. After crack formation and release from stress, the lamellar d-spacing was then recovered to a similar value as that of the film without stretching. Moreover, the compressive strain, perpendicular to the stretching direction, is also experienced by the polymer thin film, but has a magnitude that is not as large as the magnitude of the applied stretching strain. As a result, it is reasonable that the

lamellar in-plane d-spacing increases via stretching, but, the out-of-plane lamellar distance, π-π stacking distance, and edge-on configuration are preserved during stretching – consistent with our observation. For edge-on configuration, although the π-π stacking direction is also parallel to applied strain, the ordering of π-π stacking crystallites are believed to be preserved during stretching.(vide infra). This deformation behavior may be explained by the simulation of semi-crystalline polymers by Barrat et al, which suggests that when applied with uniaxial strain, the crystalline regions are affected at first and then the amorphous regions are deformed at larger strains.[38] As a result, we proposed a common model for stretching semi-crystalline conjugated polymer thin films: the crystalline region are slightly destroyed if its crystallites contain face-on configurations. And during stretching, the applied strain would be dissipated in amorphous regions and give rise to cracks. After crack propagation, the stretching polymer films are released from strain and the crystalline packing are preserved.

The coherence lengths (L_c) of out-of-plane (200) diffraction peak and in-plane π-π stacking diffraction peaks at each strain were calculated to see if there is a correlation between the crystallite size and applied strain.[39] Table S1 and Figures S11 b & c show L_c of the three polymers at different strain for out-of-plane (200) (L_c (200)) and in-plane π-π stacking (L_c (π-π)), respectively. First, the L_c (200) diffraction patterns

of P2 and P3 decreased before cracks formed, but they subsequently recovered after cracks were formed, revealing that the ordered crystallites were disturbed by strain, but once strain was released, the can recover. On the other hand, the L_c (200) of P1 kept decreasing. Interestingly, the L_c (π-π) of P1 and P3 did not change during stretching. For P2, L_c (π-π) grew slightly near the crack-onset point but recovered to the original value after being released. However, the L_c (π-π) change at different strains is much smaller than L_c (200), indicating that the ordering of π-π stacking is less effected than the ordering of the out-of-plane lamellar packing during stretching. This behavior seems reasonable since the weaker alkyl chain aggregated regions are expected to be more easily distorted than the stronger π-π stacking by strain. Consequently, the stretchability improvement via incorporation of the thiophene spacers may be due to the fact that the mixed packing structure of P2 is more susceptible to be influenced by applied strain than P3.

Conclusion

The physical, electrical, and morphological properties of conjugated polymers based on fused thiophene diketopyrrolopyrrole were characterized to elucidate how the thin film behavior under various stretching conditions depended on polymer chemical building blocks. The polymer structures were designed to vary side chains

and thiophene spacers, to enable systematic evaluation of the intrinsic ductility and elastic behavior. Introducing of branched alkyl side chains was observed to shift the thermal transitions below room temperature. The stretched polymer thin films possess different charge carrier mobilities and film morphologies. Polymers with branched alkyl side chains exhibited lower tensile moduli and later onset of crack propagation, which we attribute to the presence of softer amorphous regions than in the polymers without branched alkyl side chains. For the two polymers with branched alkyl side chains, the one with additional thiophenes inserted in polymer main chain, showed edge-on backbone configuration and an entangled nano-fibrillar texture. This polymer exhibited a delayed onset of crack propagation (40% strain). It maintained a mobility of 1×10^{-1} $cm^2 V^{-1}s^{-1}$ even when 100% strain was applied. The edge-on packing, where long axes of the alkyl chains are perpendicular to the applied stress, contributed to better mechanical compliance than the polymer exhibiting bimodal crystallite orientation. The applied stress parallel to the face-on packing plane was observed to have reduced crystallite size, resulting in the poor electrical performance under strain.

Experimental section

Materials: All processing solvents, such as chlorobenzene, were purchased from Sigma-Aldrich and used as received. The three studied

Poly(tetrathienoacene-diketopyrrolopyrrole) polymers were provided by Corning Incorporated.[27] Poly(dimethylsiloxane) (PDMS), Sylgard 184, Dow Corning, was prepared at ratios of 10:1 and 20:1 (base:crosslinker, w/w) and cured for 12 hours at 120 °C and used for the laminating substrate to transfer the polymer thin films.[40]

Preparation of semiconducting layer: Highly n-doped Si (100) wafers were cut into small pieces (2 cm × 2 cm). The wafers were cleaned with compressed air and washed with toluene, acetone, and isopropanol, in that order. The cleaned Si wafers were then modified with an octadecyltrimethoxysilane (OTS) self-assembled monolayer according to our reported method.[38,42] The polymer solutions were prepared in chlorobenzene at a concentration of 5 mg/mL. These solutions were dropped onto the OTS-treated Si substrate, spin-coated at 1000 rpm for 1 min, then annealed at 190 ^{o}C under nitrogen atmosphere for 1 hour. The thickness of the polymer films, as measured by a profilometry, were found from 30 to 400 nm controlled by solution concentration.

Characterization of transferred polymer thin film: The polymer thin films were laminated with 20:1 PDMS substrate and peeled off from OTSY-treated Si substrate. The films on PDMS substrates were transferred to a second Si substrate for further characterization. These transferred thin films were examined using a Leica DM4000M optical microscope and tapping mode atomic force microscopy (AFM). Dynamic

mechanical analysis (DMA) and differential scanning calorimetry (DSC) measurements were performed under a nitrogen atmosphere at a heating rate of 10^{o}C/min by using a TA instruments Q-800 and a Q-2000, respectively. Grazing incidence X-ray diffraction (GIXD) experiment was performed at the Stanford Synchrotron Radiation Lightsource (SSRK) at beamline 11–3 with a photon energy of 12.735 KeV and sample to detector distance of ~400mm. The incidence angle was fixed at 0.12° to enhance the diffraction intensity and reduce the substrate scattering. Numerical integration of the diffraction peak areas was performed with the software WxDiff.[43] The transferred thin films on silicon substrate with thermally grown 300 nm SiO_2 layers were directly evaporated with gold electrodes (40 nm) with a channel length (L) of 50 μm, and a channel width (W) of 1000 μm, to give a top-contact/bottom gate field-effect-transistor architecture.

Buckling-Based Method:[32] The 10:1 PDMS was cut into rectangular pieces and stretched to strains of 4% using a computer-controlled stage, which applied strain to samples by using a linear actuator. The conjugated polymer films were transferred from OTSY-treated Si substrate to the pre-strained PDMS substrate in one fast motion after applying a minimum amount of pressure. Buckles formed in the conjugated polymer films upon relaxation of the substrate and were visualized using a Leica DM4000M optical microscope to measure the buckling wavelength.

Acknowledgements

C. Lu acknowledge support the National Science Council of Taiwan for financial support (NSC 103-2917-I-002-165). Z.Bao acknowledge support from the Air Force Office of Scientific Research (FA9550-15-1-0106) and Samsung Electronics. Use of the Stanford Synchrotron Radiation Lightsource, SLAC National Accelerator Laboratory, is supported by the U.S. Department of Energy, Office of Science, Office of Basic Energy Sciences under Contract No. DE-AC02-76SF00515.

Reference

(1) Savagatrup, S.; Printz, A. D.; O'Connor, T. F.; Zaretski, A. V.; Lipomi, D. J. *Chem. Mater.* **2014**, *26*, 3028.

(2) O'Connor, B.; Kline, R. J.; Conrad, B. R.; Richter, L. J.; Gundlach, D.; Toney, M. F.; DeLongchamp, D. M. *Adv. Funct. Mater.* **2011**, *21*, 3697.

(3) Chortos,A.;Lim, J.;To, J. W. F. ;Vosgueritchian, M.;Dusseault, T. J.;Kim, T.-H.; Hwang, S; Bao, Z. *Adv. Mater.* **2014**, *26*, 4253.

(4) Shin, M.; Oh,J.-Y.;Byun, K.-E.; Lee Y.-J.; Kim, B.;Baik, H.-K. ;Park, J.-J.;Jeong, U. *Adv. Mater.* **2015**, *27*, 1255.

(5) Savagatrup, S.; Makaram, A. S.; Burke, D. J.; Lipomi, D. J. *Adv. Funct. Mater.* **2014**, *24*, 2264.

(6) Lipomi, D. J.; Chong, H.; Vosgueritchian, M.; Mei, J.; Bao, Z. *Sol. Energy Mater. Sol. Cells* **2012**, *107*, 355.

(7) O'Connor, B.; Chan, E. P.; Chan, C.; Conrad, B. R.; Richter, L. J.; Kline, R. J.; Heeney, M.; McCulloch, I.; Soles, C. L.; DeLongchamp, D. M. *ACS Nano* **2010**, *4*, 7538.

(8) Rogers, J. A.; Someya, T.; Huang, Y. G. *Science* **2010**, *327*, 1603.

(9) Sekitani, T.; Someya, T. *Adv. Mater.* **2010**, *22*, 2228.
(10) McCulloch, I.; Heeney, M.; Chabinyc, M. L.; DeLongchamp, D.; Kline, R. J.; Cölle, M.; Duffy, W.; Fischer, D.; Gundlach, D.; Hamadani, B.; Hamilton, R.; Richter, L.; Salleo, A.; Shkunov, M.; Sparrowe, D.; Tierney, S.; Zhang, W. *Adv. Mater.* **2009**, *21*, 1091.
(11) Pistor, V.; de Conto, D.; Ornaghi, F. G.; Zattera, A. J. *J. Nanomater.* **2012**, http://dx.doi.org/10.1155/2012/283031.
(12) Schönherr, H.; Wiyatno, W.; Pople, J.; Frank, C. W.; Fuller, G. G.; Gast, A. P.; Waymouth, R. M. *Macromolecules* **2002**, *35*, 2654.
(13) Fu, B.; Baltazar, J.; Sankar, A. R.; Chu, P.-H.; Zhang, S.; Collard, D. M.; Reichmanis, E. *Adv. Funct. Mater.* **2014**, *24*, 3734.
(14) Kanimozhi, C.; Yaacobi-Gross, N.; Burnett, E. K.; Briseno, A. L.; Anthopoulos, T. D.; Salzner, U.; Patil, S. *Phys. Chem. Chem. Phys.* **2014**, *16*, 17253.
(15) Nofar, M.; Zhu, W.; Park, C. B.; Randall, J. *Ind. Eng. Chem. Res.* **2011**, *50*, 13789.
(16) Lieser, G.; Oda, M.; Miteva, T.; Meisel, A.; Nothofer, H.-G.; Scherf, U.; Neher, D. *Macromolecules* **2000**, *33*, 4490.
(17) Jin, Y. J.; Bae, J. E.; Cho, K. S.; Lee, W. E.; Hwang, D. Y.; Kwak, G. *Adv. Funct. Mater.* **2014**, *24*, 1928.
(18) Savagatrup, S.; Printz, A. D.; Rodriquez, D.; Lipomi, D. J. *Macromolecules* **2014**, *47*, 1981.
(19) Kline, R. J.; DeLongchamp, D. M.; Fischer, D. A.; Lin, E. K.; Richter, L. J.; Chabinyc, M. L.; Toney, M. F.; Heeney, M.; McCulloch, I. *Macromolecules* **2007**, *40*, 7960.
(20) Mei, J.; Bao, Z. *Chem. Mater.* **2014**, *26*, 604.
(21) Jin, Y.-J.; Bae, J.-E.; Cho, K.-S.; Lee, W.-E.; Hwang, D.-Y.; Kwak, G. *Adv. Funct. Mater.* **2014**, *24*, 1928.
(22) Gargi, D.; Kline, R. J.; DeLongchamp, D. M.; Fischer, D. A.; Toney, M. F.; O'Connor, B. T. *J. Phys. Chem. C*, **2013**, *117*, 17421.
(23) O'Connor, B. T.; Reid, O. G.; Zhang, X.; Kline, R. J.; Richter, L. J.; Gundlach, D. J.; DeLongchamp, D. M.; Toney, M. F.; Kopidakis, N.; Rumbles, G. *Adv. Funct. Mater.* **2014**, *24*, 3422.
(24) Chen, M. S.; Niskala, J. R.; Unruh, D. A.; Chu, C. K.; Lee, O. P.; Fréchet, J. M. J. *Chem. Mater.* **2013**, *25*, 4088.
(25) Zhang, X.; Richter, L. J.; DeLongchamp, D. M.; Kline, R. J.; Hammond, M. R.; McCulloch, I.; Heeney, M.; Ashraf, R. S.; Smith, J. N.; Anthopoulos, T. D.; Schroeder, B.; Geerts, Y. H.; Fischer, D. A.; Toney, M. F. *J. Am. Chem. Soc.* **2011**, *133*, 15073.
(26) Wu, W.; Liu, Y.; Zhu, D. *Chem. Soc. Rev.* **2010**, *39*, 1489.

(27) Matthews, J. R.; Niu, W.; Tandia, A.; Wallace, A. L.; Hu, J.; Lee, W.-Y.; Giri, G.; Mannsfeld, S. C. B.; Xie, Y.; Cai, S.; Fong, H. H.; Bao, Z.; He, M. *Chem. Mater.* **2013**, *25*, 782.
(28)Lee, J. S.; Son, S. K.; Song, S.; Kim, H.; Lee, D. R.; Kim, K.; Ko, M. J.; Choi, D. H.; Kim, B.; Cho, J. H. *Chem. Mater.* **2012**, *24*, 1316.
(29)Perez, L. A.; Zalar, P.; Ying, L.; Schmidt, K.; Toney, M. F.; Nguyen, T.-Q.; Bazan, G. C.; Kramer, E. J. *Macromolecules* **2014**, *47*, 1403.
(30) Lee, W.-Y.; Giri, G.; Diao, Y.; Tassone, C. J.; Matthews, J. R.; Sorensen, M. L.; Mannsfeld, S. C. B.; Chen, W.-C.; Fong, H. H.; Tok, J. B. H.; Toney, M. F.; He, M.; Bao, Z. *Adv. Funct. Mater.* **2014**, *24*, 3524.
(31) Akabori, K.-i.; Tanaka, K.; Nagamura, T.; Takahara, A.; Kajiyama, T. *Macromolecules* **2005**, *38*, 9735.
(32) Tahk, D.; Lee, H. H.; Khang, D.-Y. *Macromolecules* **2009**, *42*, 7079.
(33) Breese, D. R.; Beaucage, G. *J. Polym. Sci., Part B: Polym. Phys.* **2008**, *46*, 607.
(34) Toney, M.F.; Brennan, S. *Phys. Rev. B* **1989**, *39*, 7963.
(35)Atrazhev, V. V; Burlatsky, . F;Dmitriev, D. V;Sultanov. V. I *J. Stat. Mech. Theor. Exp.* **2013**, *02* , P02004.
(36) Rivnay, J.; Mannsfeld, S. C. B.; Miller, C. E.; Salleo, A.;Toney, M. F. *Chem. Rev.* **2012**, *112*, 5488.
(37) Toki, S.; Sics, I.; Ran, S.; Liu, L.; Hsiao, B. S. *Polymer* **2003**, *44*, 6003.
(38) Jabbari-Farouji, S.;Rottler, J. ;Lame, O.;Makke, A. ;Perez, M.;Barrat, J.-L. *J. Phys. Condens. Matter* **2015**, *27*, 194131.
(39) Rivnay, J.; Noriega, R.; Kline, R. J.; Salleo, A.; Toney, M. F. *Phys. Rev. B* **2011**, *84*, 045203.
(40) Reese, C.; Chung, W. J.; Ling, M. M.; Roberts, M.; Bao, Z. N. *Appl. Phys. Lett.* **2006**, *89*.
(41) Virkar, A.; Mannsfeld, S.; Oh, J. H.; Toney, M. F.; Tan, Y. H.; Liu, G.-y.; Scott, J. C.; Miller, R.; Bao, Z. *Adv. Funct. Mater.* **2009**, *19*, 1962.
(42) Ito, Y.; Virkar, A. A.; Mannsfeld, S.; Oh, J. H.; Toney, M.; Locklin, J.; Bao, Z. *J. Am. Chem. Soc.* **2009**, *131*, 9396.
(43) Mannsfeld, S. C. B.; Tang, M. L.; Bao, Z. *Adv. Mater.* **2011**, *23*, 127.

Table 1. The d-spacing of lamellar and ***π-π*** packing of our polymers before and after crack propagation

	Molecular	**weight**	**Lamellar**		**packing**		***π-π***		**stacking**	
	M_w	**PD**	**d-sp**	**d-spa**	**d-spac**	**d-spac**	**d-sp**	**d-spa**	**d-spac**	**d-spac**

		I	acing (Å)	cing duri ng stret ching (Å)	ing near crack propa gation (Å)	ing after crack propa gation (Å)	acing (Å)	cing duri ng stret ching (Å)	ing near crack propa gation (Å)	ing after crack propa gation (Å)
P 1	44.2k	1.9 4	26.97	-	27.12	27.2	3.66	-	3.66	3.66
P 2	32.7k	1.7 5	25.86 [a] /24.9 3[b]	25.94 [a] / 25.23 [b]	26.22[a] /26.09[b]	25.85[a] /24.83[b]	3.81	3.83	3.83	3.82
P 3	49.8k	1.6 9	23.62	23.57	23.57	23.65	3.73	3.71	3.72	3.72

The lamellar d-spacing in [a] out of plane direction and [b] in plane direction. And the crack-onset points of P1, P2 ,and P3 are near 10%, 20%, 40% strain, respectively.

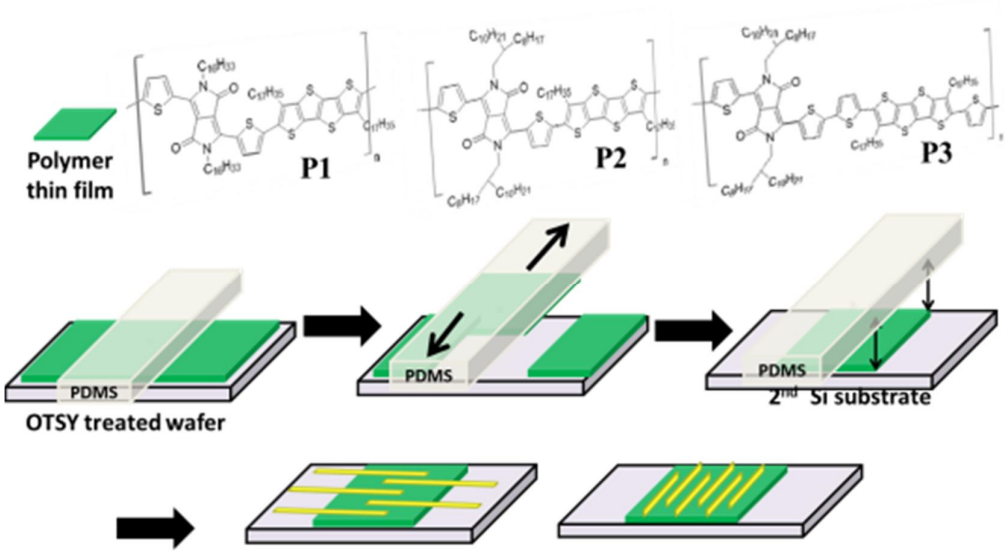

Figure 1. The chemical structures of the fused thiophene diketopyrrolopyrrole-based polymers and a schematic of the stretching and transferring process.

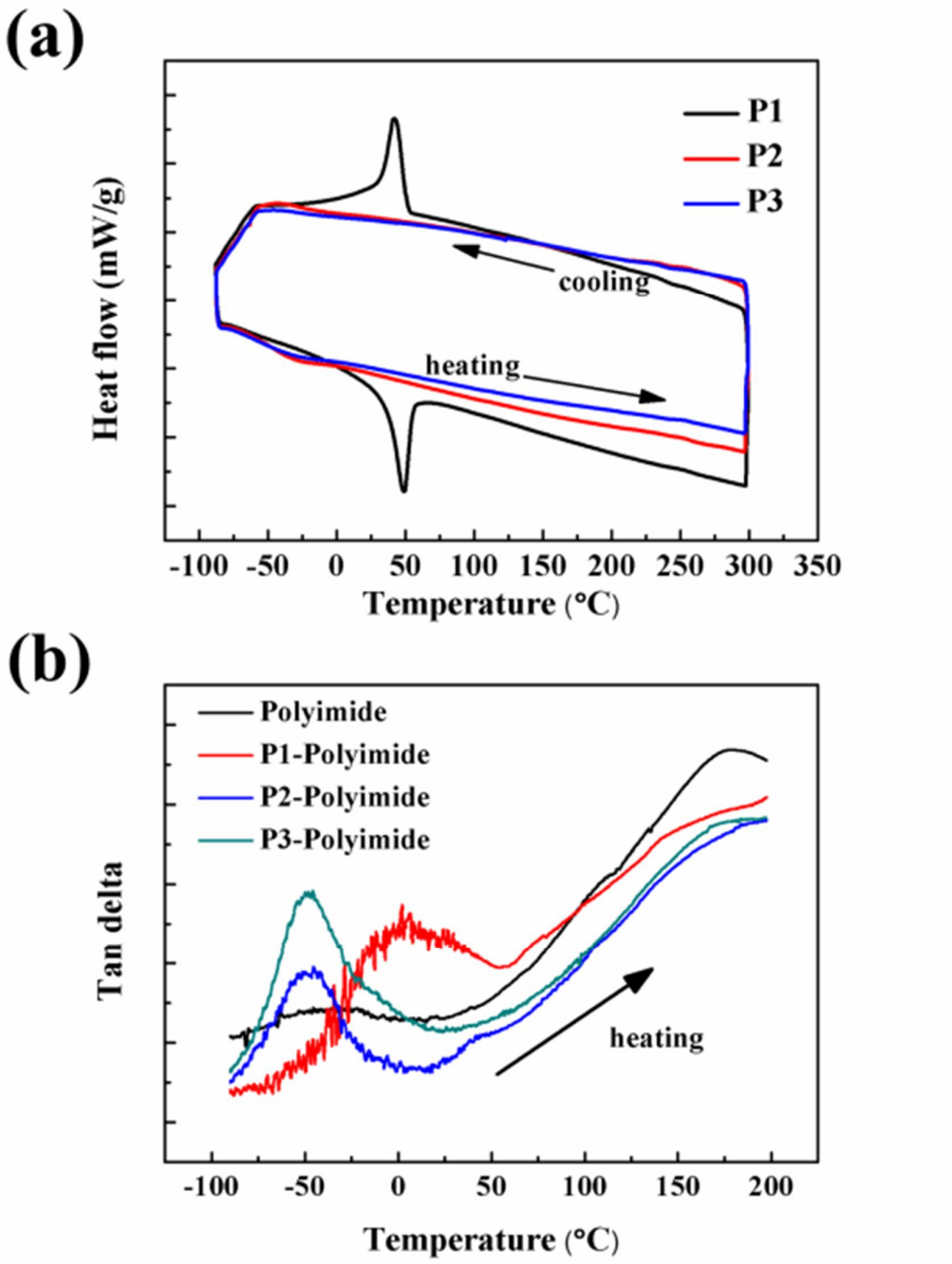

Figure 2. (a) DSC thermogram of the studied polymers at heating/cooling rate of 10 °C/min, (b) DMA curves of samples at frequency of 1 Hz and heating rate of 10 °C/min.

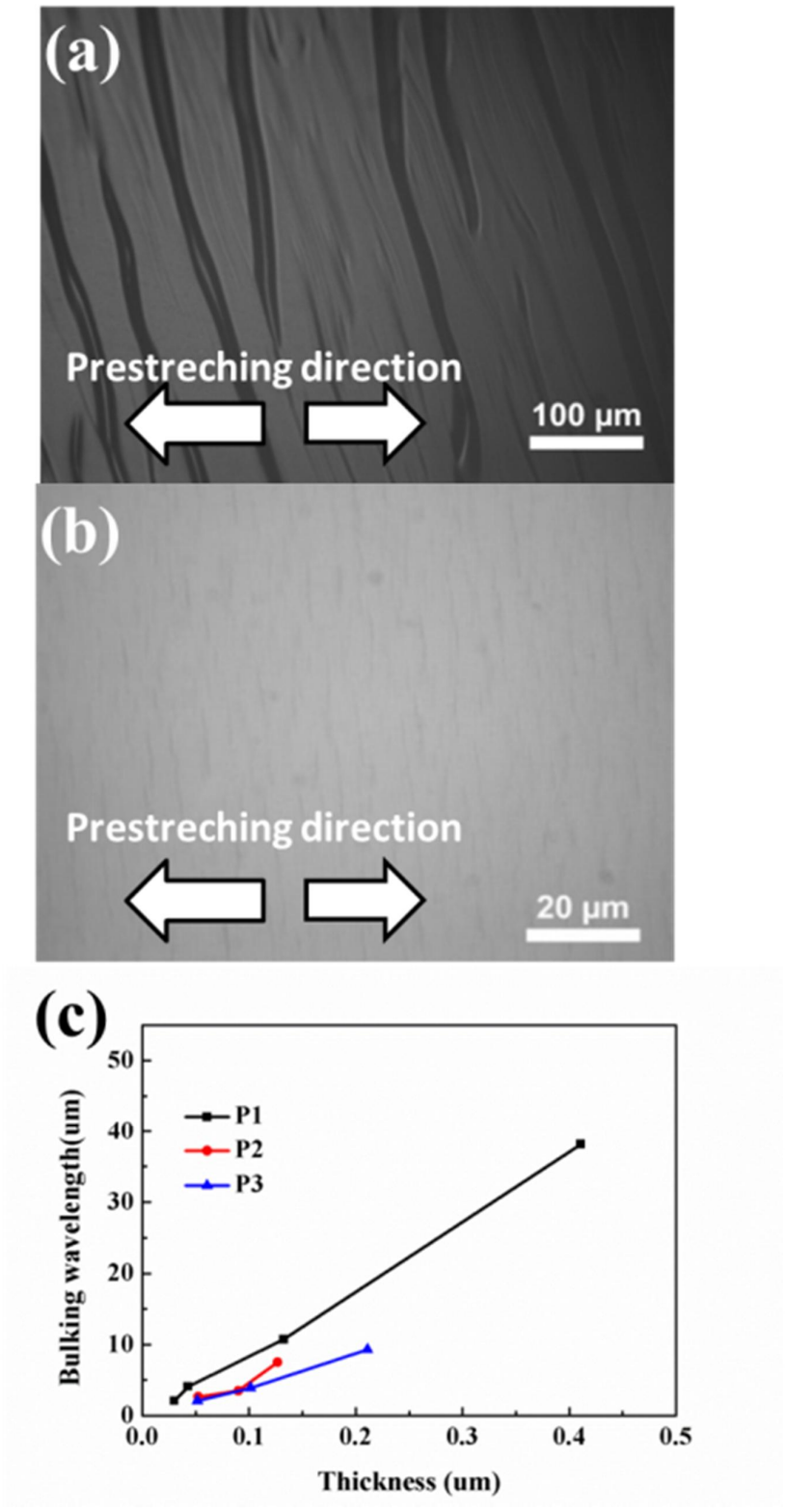

Figure 3. Mechanical properties of the three studied polymers. Optical micrographs of buckled films of a) P1 with λ_b= 38.1 μm and d_f = 410nm and (b) P3 with λ_b = 3.93 μm and d_f = 101 nm; (c) buckling wavelength *vs*. film thickness.

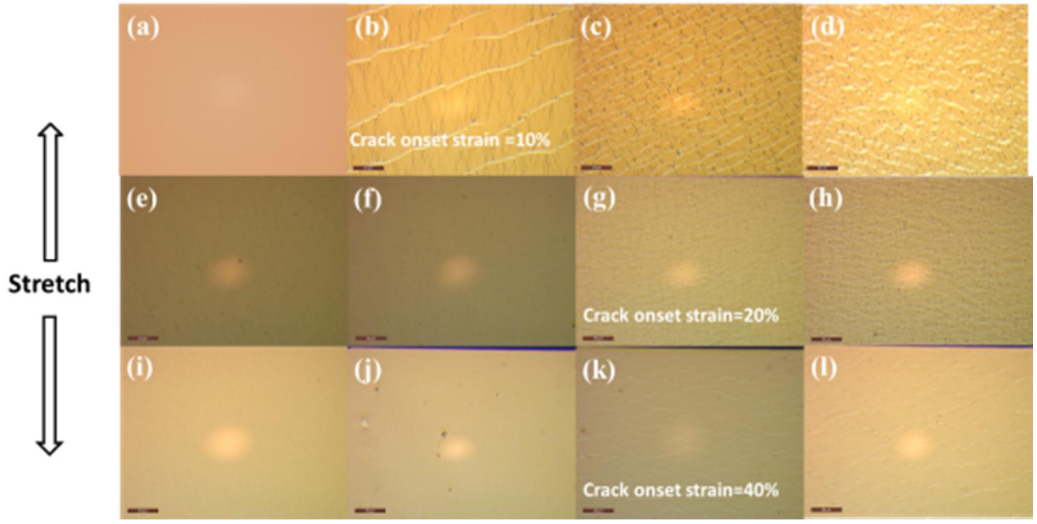

Figure 4. Optical micrographs of thin films of P1 with (a) 0%, (b) 10%, (c) 20%, (d) 50% strain, P2 with (e) 0%, (f) 10%, (g) 20%, (h) 50% strain ,and P3 with (i) 0%, (j) 30%, (k) 40%, (l) 50% strain.

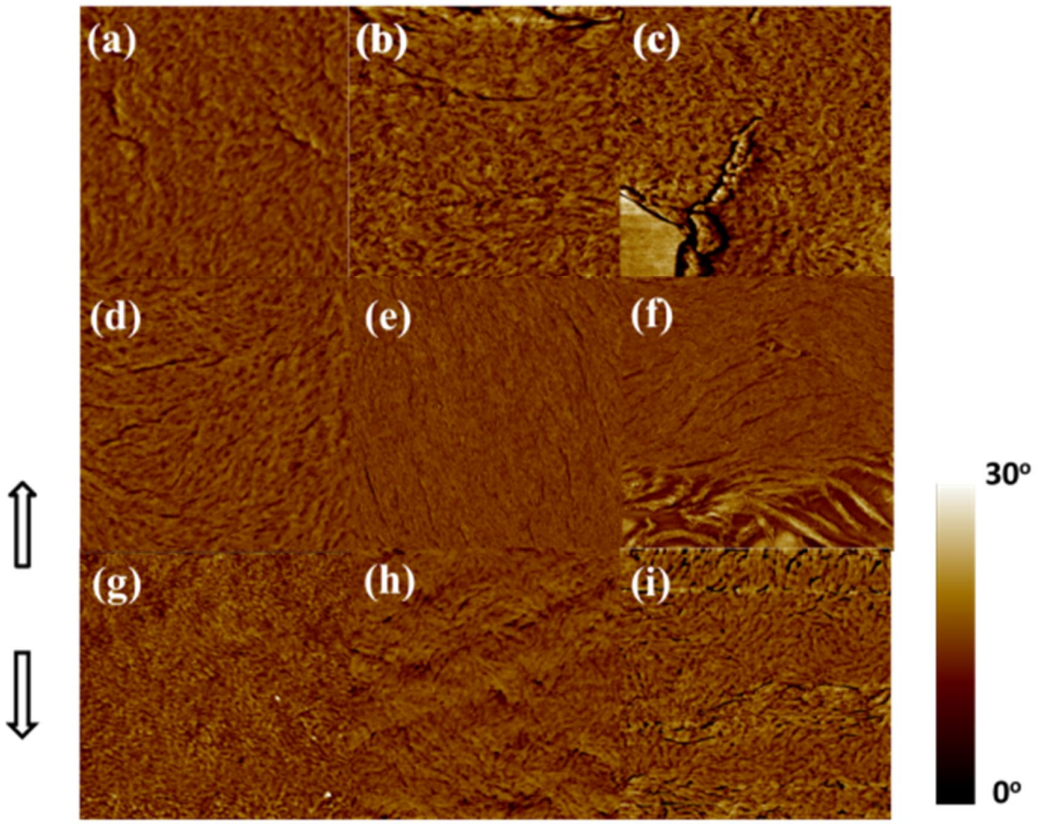

Figure 5. AFM phase images of the polymer thin films: P1 at (a) 0%, (b) 20%, and (c) 50% strain, P2 at (d) 0%, (e) 20%, and (f) 50% strain, and P3 at (a) 0%, (b) 20%, and (c) 50% strain in 1μm×1μm scale.

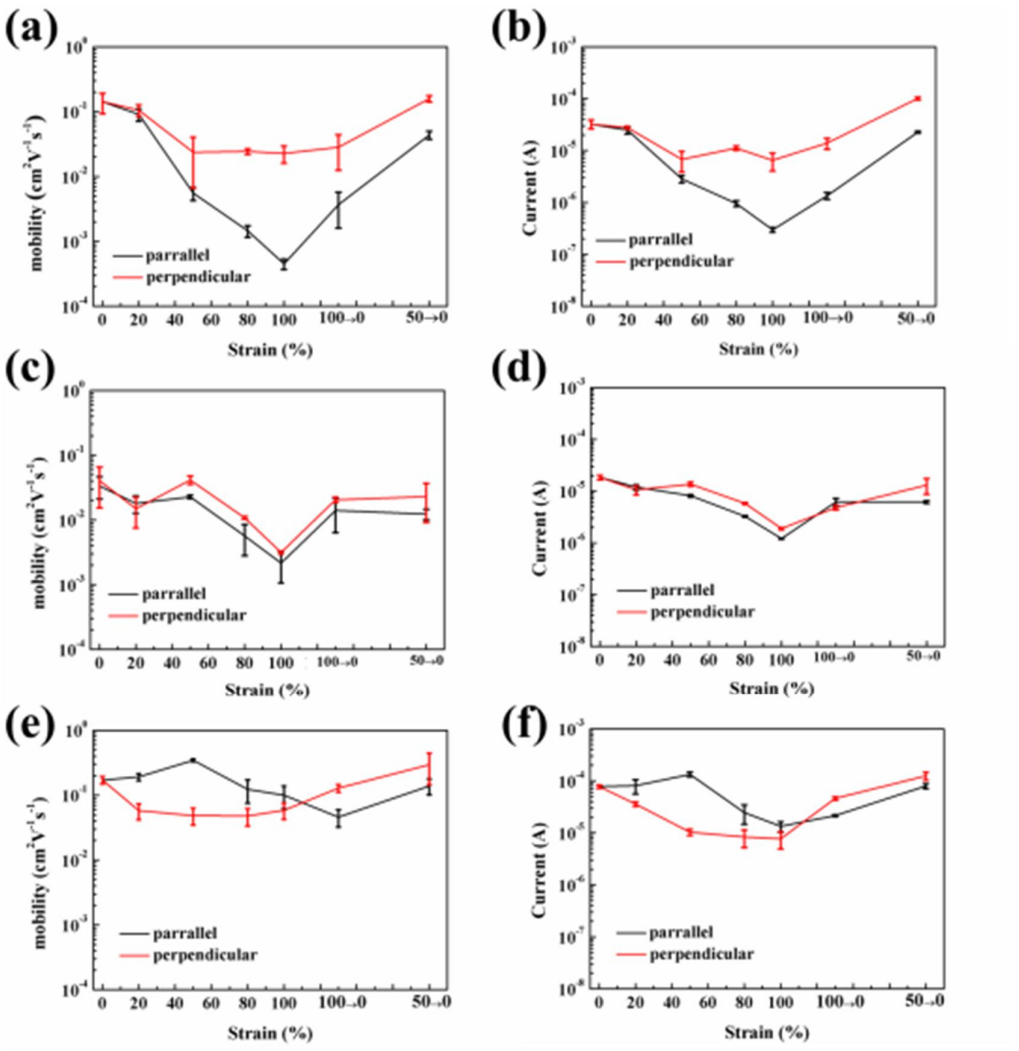

Figure 6. The mobilities of (a) P1,(c) P2 and (e) P3, and the on currents of (b) P1,(d) P2 and (f) P3 polymer thin films at different strains for transistors with 50 μm channel length.

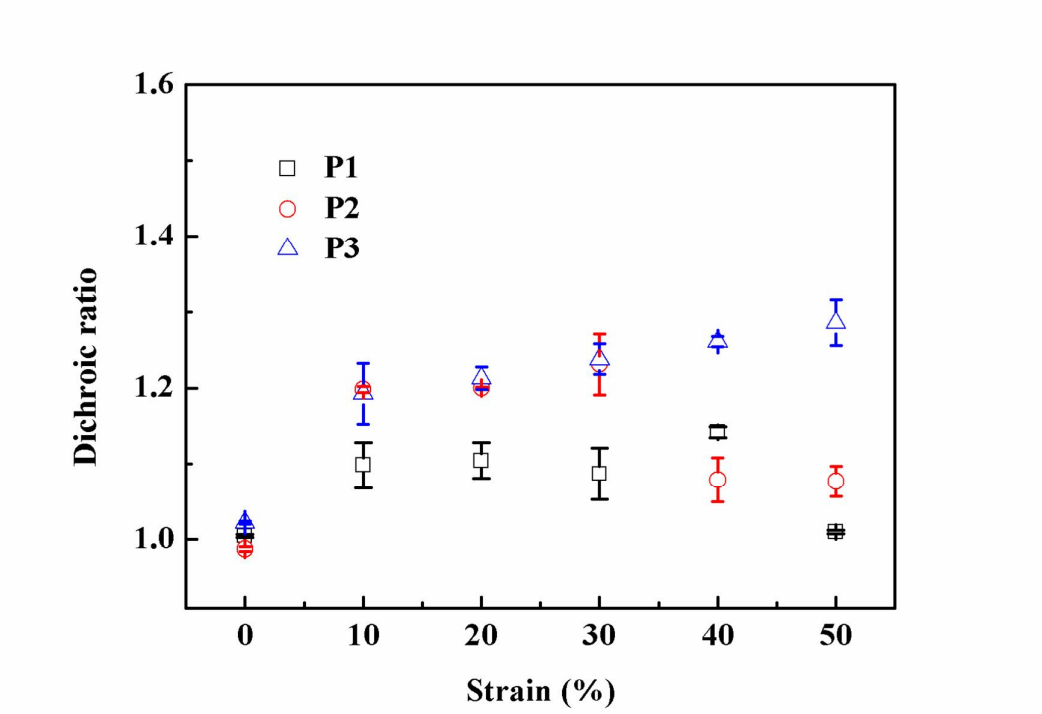

Figure 7. Dichroic ratios (R) of the studied polymers under different amounts of applied strain.

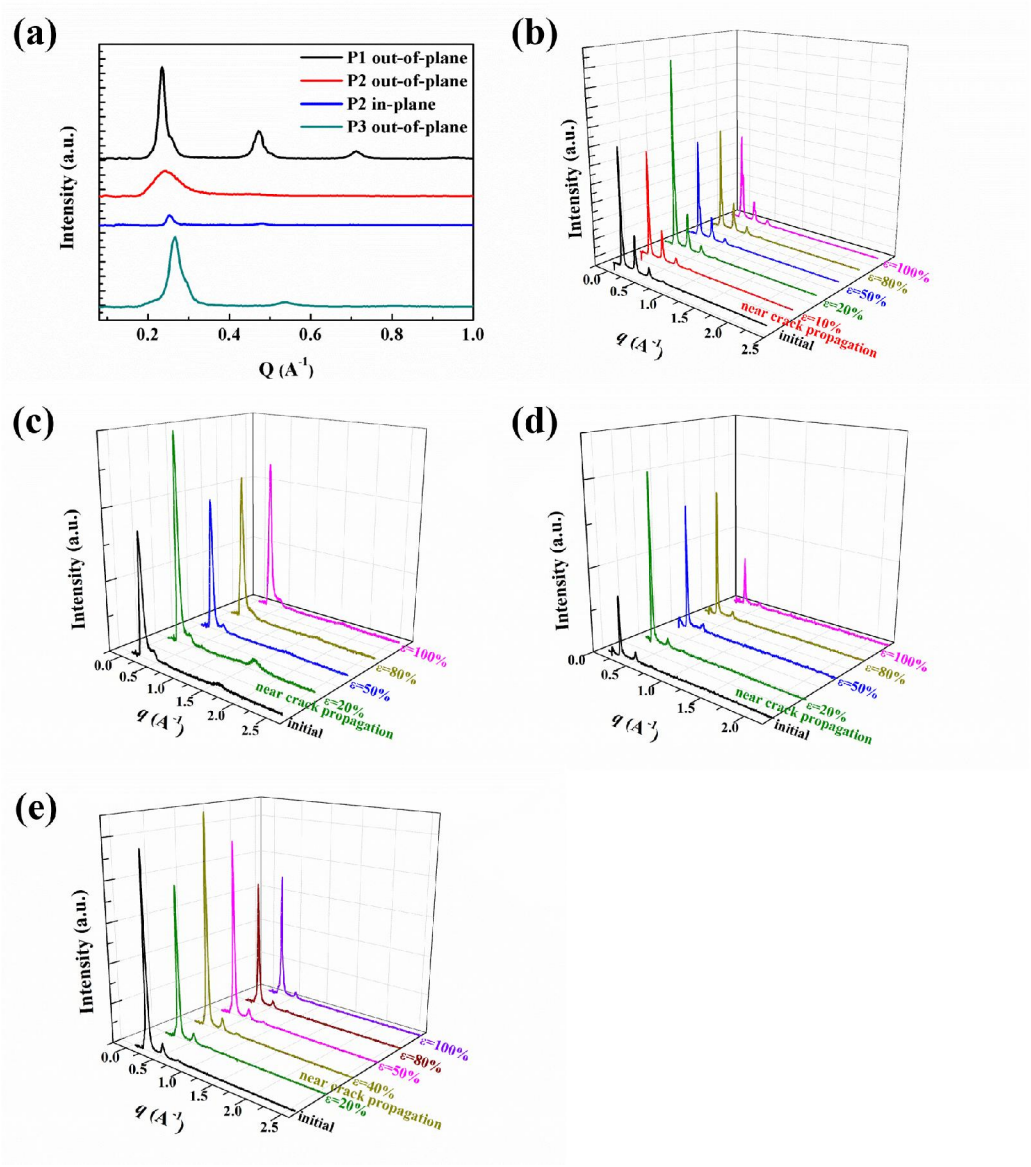

Figure 8. The GIXD profiles of (a) polymers without strain, (b) P1 (out-of-plane), (c) P2 (out-of-plane), (d) P2 (in-plane), and (e) P3 (out-of-plane) at different applied strains. Note that the crack onset strains are 10%, 20%, and 40% for P1, P2, and P3, respectively.

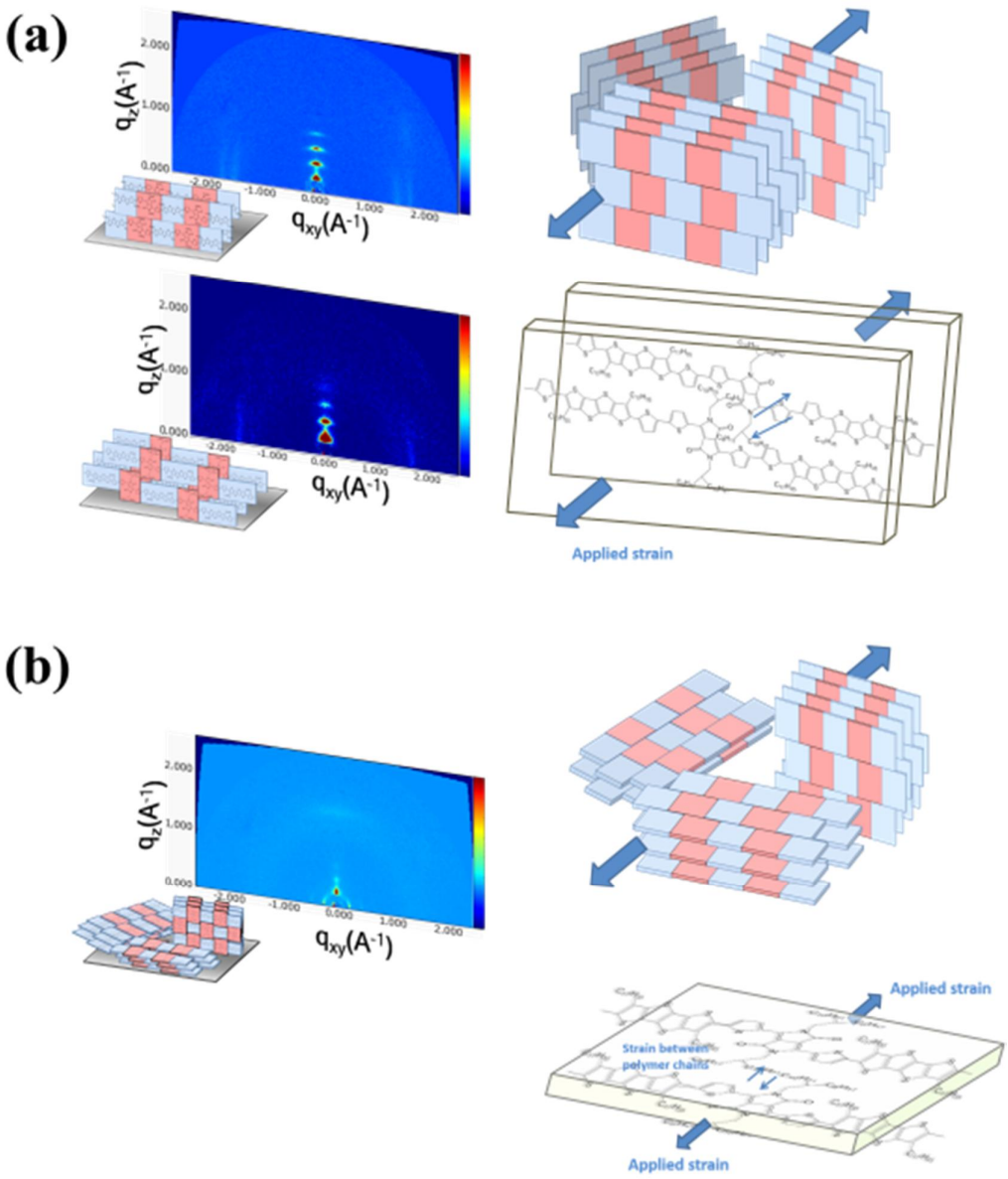

Figure 9. A schematic representation of the crystalline packings of (a) P1 and P3, (b) P2 with applied strain in crystalline domains and between polymer chains

Supplementary Information

Effects of Molecular Structure and Packing Order on the Stretchability of Semi-Crystalline Conjugated Poly(tetrathienoacene-diketopyrrolopyrrole) Polymers

Chien Lu, Wen-Ya Lee, Xiaodan Gu, Jie Xu, Ho-Hsiu Chou, Hongping Yan, Mingqian He, James R Matthews, Weijun Niu, Wen-Chang Chen and Zhenan Bao*

[*]Chien Lu, Dr. Xiaodan Gu, , Dr. Jie Xu, Dr. Ho-Hsiu Chou, Dr. Jeffery B.-H. Tok, Prof. Z. Bao
Department of Chemical Engineering, Stanford University
Stanford, California 94305, United States
E-mail: zbao@stanford.edu

Prof. W.-Y. Lee
Department of Chemical Engineering and Biotechnology,

National Taipei University of Technology, Taipei 106, Taiwan

Dr. Hongping Yan and Prof. Michael F. Toney
Stanford Synchrotron Radiation Lightsource, SLAC National Accelerator Laboratory, Menlo Park, California 94025, United States

Dr. Mingqian. He, Dr. James R Matthews, Dr. Weijun Niu
Corning Incorporated, One River Front Plaza,
Corning, New York 14831, United States

Chien Lu, Prof. W.-C. Chen
Department of Chemical Engineering, National Taiwan University
Taipei, 10617 Taiwan

Synthesis of monomers, P2 ,and P3

3,6-bis(5-bromothiophen-2-yl)-2,5-bis(2-octyldodecyl)pyrrolo[3,4-c]pyrrole-1,4(2H,5H)-dione(A):[1] ^{1}H NMR (300 MHz, $CDCl_2$) δ 8.48 (d, 2H), 7.16 (d, 2H), 3.83 (d, 4H), 1.85-1.73 (m, 2H), 1.31-1.05 (m, 64H), 0.86-0.76 (m, 12H). Anal. Calcd for $C_{54}H_{86}Br_2N_2O_2S_2$: C, 63.64; H, 8.50; N, 2.75; Found: C, 63.22; H, 8.46N, 2.42.

3,7-diheptadecylthieno[2',3':4,5]thieno[3,2-b]thieno[2,3-d]thiophene-2,6-diyl)bis(trimethylstannane)(B):[2] ^{1}H NMR (CD_2Cl_2, 300 MHz) 0.44 (18H, s), 0.88 (6H, t, J = 7.5), 1.18 – 1.47 (56H, m), 1.67 – 1.80 (4H, m), 2.75 (4H, t, J = 7.5); įC (CD2Cl2, 75 MHz) -7.67 (6C), 14.28 (2C), 23.11 (2C), 29.77 (2C), 29.88 (2C), 29.94 (2C), 30.10 (20C), 30.51 (2C), 32.35 (2C), 132.60 (2C), 134.78 (2C), 137.01 (2C), 142.98 (2C), 143.22 (2C); m/z (APCI+) 1054.04 [M+H]+ ; Anal. Calc. for C50H88S4Sn2: C, 56.93; H, 8.41. Found: C, 57.18; H, 8.17.

(5,5'-(3,7-diheptadecylthieno[2',3':4,5]thieno[3,2-b]thieno[2,3-d]thiophene-2,6-di

yl)bis(thiophene-5,2-diyl))bis(trimethylstannane)(C): To Compound D (2.78 g, 3.11 mmol) in 200 mL of anhydrous THF at -78°C, n-BuLi (2.0 M in hexane) (4.6 mL, 9.2 mmol) was added dropwise. The resulting solution was allowed to warm to room temperature and stirred for 4 h. It was then cooled to -78°C and Me_3SnCl solution (1 M in THF) (12.48 mL, 12.48 mmol) was added dropwise. The cloudy reaction solution was allowed to warm to room temperature and stirred overnight. 100 mL of ice-water was added into the cloudy solution and THF was removed under reduced pressure to yield a light yellowish solid in aqueous suspension. The solid was filtered from the aqueous phase and dissolved in ethyl acetate, then washed by water and dried over Na_2SO_4 (anhydrous). After the evaporation of solvent, the residue was recrystallized twice from a mixed solvent system acetone/ethyl acetate (3:1) to form the desired product Compound C as a light yellow solid (2.69 g, 71%). ^{1}H NMR (300 MHz, CD_2Cl_2): δ 7.23 (d, J = 3.0 Hz, 2H), 7.12 (d, J = 3.0 Hz, 2H), 2.86 (t, J = 9.0 Hz, 4 H), 1.72 (p, J =6.0 Hz, 4 H), 1.43-1.09 (m, 56 H), 0.80 (t, J = 6.0 Hz, 6 H), 0.35 (s, 18 H). Anal. Calcd for $C_{58}H_{92}S_6Sn_2$: C, 57.14; H, 7.61; Found: C, 57.43; H, 7.89.

Poly-3-(5-(3,7-diheptadecyl-6-methylthieno[2',3':4,5]thieno[3,2-b]thieno[2,3-d]thiophen-2-yl)thiophen-2-yl)-6-(5-methylthiophen-2-yl)-2,5-bis(2-octyldodecyl)pyrrolo[3,4-c]pyrrole-1,4(2H,5H)-dione (P2)

To a 35 mL microwave reaction vessel equipped with a magnetic stir bar were added 2,6-di(trimethylstannyl)-3,7-diheptadecylthieno[3,2-b]thieno[2',3':4,5]thieno[2,3-d]thiophene (1g, 0.948 mmol, compound B), 3,6-bis(5-bromothiophen-2-yl)-2,5-bis(2-octyldodecyl)pyrrolo[3,4-c]pyrrole-1,4(2H,5

H)-dione (0.966g, 0.948 mmol, compound A), tris(dibenzylideneacetone)dipalladium(0) (17.3 mg, 18.9 mol) and o-tolyl phosphine (23.0 mg, 75.6 mol). The reaction vessel and cap were introduced into a nitrogen glovebox, where toluene (20 mL) was added and the cap affixed to the vessel. The vessel was then removed from the glovebox and the reaction microwaved at 160 °C for 2 h. The mixture was cooled to 50 °C before release from the microwave reactor, then poured into a stirring mixture of methanol and acetylacetone (200 mL + 200 mL). Hydrochloric acid (2 mL, 35% aq) was added and the mixture stirred for 16 h. The mixture was filtered and the polymer was placed into a glass with glass frit Soxhlet thimble. The polymer was extracted in a Soxhlet apparatus with acetone (250 mL) for 24 h, then hexanes (250 mL) for 24 h. The polymer was then extracted from the Soxhlet apparatus into chloroform (250 mL). The chloroform solution was poured into methanol (400 mL) with rapid stirring, followed by moderate stirring for 20 min. The polymer was then filtered from the mixture and dried under vacuum to give the product,

Poly-3-(5-(3,7-diheptadecyl-6-methylthieno[2',3':4,5]thieno[3,2-b]thieno[2,3-d]thiophen-2-yl)thiophen-2-yl)-6-(5-methylthiophen-2-yl)-2,5-bis(2-octyldodecyl)pyrrolo[3,4-c]pyrrole-1,4(2H,5H)-dione (Compound **04**) (1.46 g, 97.3%). Calculated repeat unit $C_{98}H_{158}N_2O_2S_6$: C, 74.18; H, 9.91; N, 1.77; Found: C, 74.31; H, 9.89; N, 1.80.

Poly -3-(5'-(3,7-diheptadecyl-6-methylthieno[2',3':4,5]thieno[3,2-b]thieno[2,3-d]thiophen-2-yl)-[2,2'-bithiophen]-5-yl)-6-(5'-methyl-[2,2'-bithiophen]-5-yl)-2,5-bis(2-octyldodecyl)pyrrolo[3,4-c]pyrrole-1,4(2H,5H)-dione (P3)

To a 15 mL microwave reaction vessel equipped with a magnetic stir bar were added (5,5'-(3,7-diheptadecylthieno[2',3':4,5]thieno[3,2-b]thieno[2,3-d]thiophene-2,6-diyl)bi

s(thiophene-5,2-diyl))bis(trimethylstannane) (0.5g, 0.41mmol, compound C), 3,6-bis(5-bromothiophen-2-yl)-2,5-bis(2-octyldodecyl)pyrrolo[3,4-c]pyrrole-1,4(2H,5H)-dione (0.42g, 0.41mmol, compound A), tris(dibenzylideneacetone)dipalladium(0) (7.50 mg, 0.0082 mol) and o-tolyl phosphine (10.00 mg, 0.0164 mol). The reaction vessel and cap were introduced into a nitrogen glovebox, where toluene (4 mL) and Butylacetate (6 mL) were added and the cap affixed to the vessel. The vessel was then removed from the glovebox and the reaction microwaved at 160 °C for 2 h. The mixture was cooled to 50 °C before release from the microwave reactor, then poured into a stirring mixture of methanol and acetylacetone (100 mL + 100 mL). Hydrochloric acid (1 mL, 35% aq) was added and the mixture stirred for 16 h. The mixture was filtered and the polymer placed into a glass with glass frit Soxhlet thimble. The polymer was extracted in a Soxhlet apparatus with acetone (250 mL) for 24 h, then hexanes (250 mL) for 24 h. The polymer was then extracted from the Soxhlet apparatus into chloroform (250 mL). The chloroform solution was poured into methanol (200 mL) with rapid stirring, followed by moderate stirring for 20 min. The polymer was then filtered from the mixture and dried under vacuum to give the product Poly -3-(5'-(3,7-diheptadecyl-6-methylthieno[2',3':4,5]thieno[3,2-b]thieno[2,3-d]thiophen-2-yl)-[2,2'-bithiophen]-5-yl)-6-(5'-methyl-[2,2'-bithiophen]-5-yl)-2,5-bis(2-octyldodecyl)pyrrolo[3,4-c]pyrrole-1,4(2H,5H)-dione (Compound **06**) (1.46 g, 97.3%). Calculated repeat unit chemical Formula: $C_{106}H_{162}N_2O_2S_8$. C, 72.71; H, 9.21; N, 1.60; Found: C, 72.64; H, 9.22; N, 1.61.

Reaction scheme of monomers and polymers

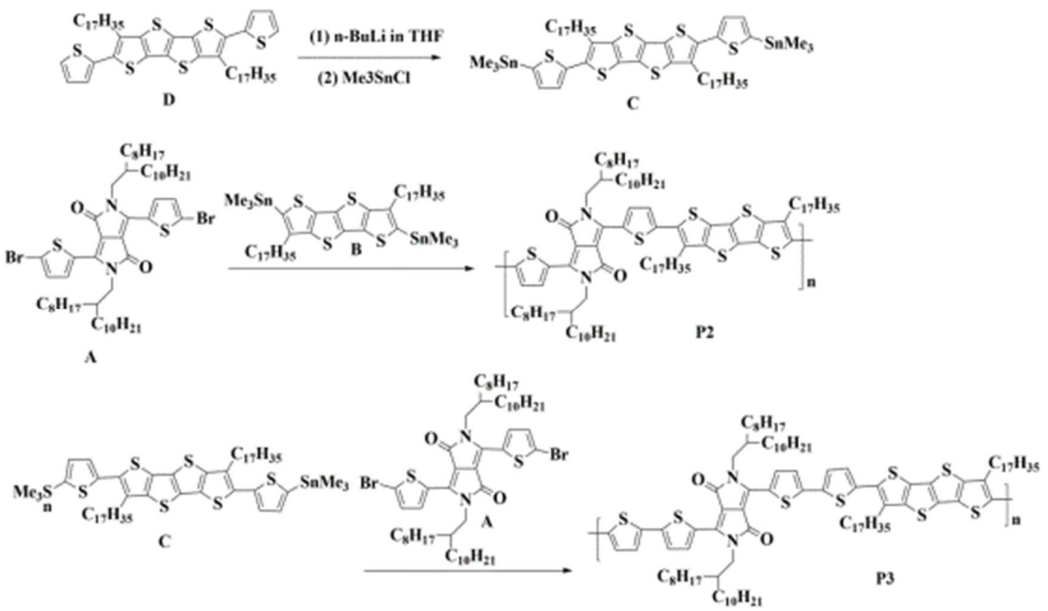

Reference:

1. Kanimozhi, C.;Yaacobi-Gross, N,;Chou, K. W.;Amassian, A.; Anthopoulos, T. D.;Patil, S., *J. Am. Chem. Soc.*, **2012**, *134* , 16532.
2. Matthews, J. R.; Niu, W.; Tandia, A.; Wallace, A. L.; Hu, J.; Lee, W.-Y.; Giri, G.; Mannsfeld, S. C. B.; Xie, Y.; Cai, S.; Fong, H. H.; Bao, Z.; He, M. *Chem. Mater.* **2013**, *25*, 782.

	Lamellar packing				*π-π* stacking			
	L_c (Å)	**L_c (Å) during stretching**	**L_c near crack propagation (Å)**	**L_c after crack propagation (Å)**	**L_c (Å)**	**L_c (Å) during stretching**	**L_c near crack propagation (Å)**	**L_c after crack propagation (Å)**
P1	87.27	-	89.19	53.05	24.25	-	18.90	20.08
P2	43.17	31.70	39.60	41.10	16.32	27.61	15.53	12.27
P3	51.04	47.20	46.43	49.87	18.29	17.34	18.87	19.05

Table S1. Coherence Length (L_c) of out-of-plane lamellar packing (200) diffractions and *π-π* stacking of the three studied polymers before and after crack propagation

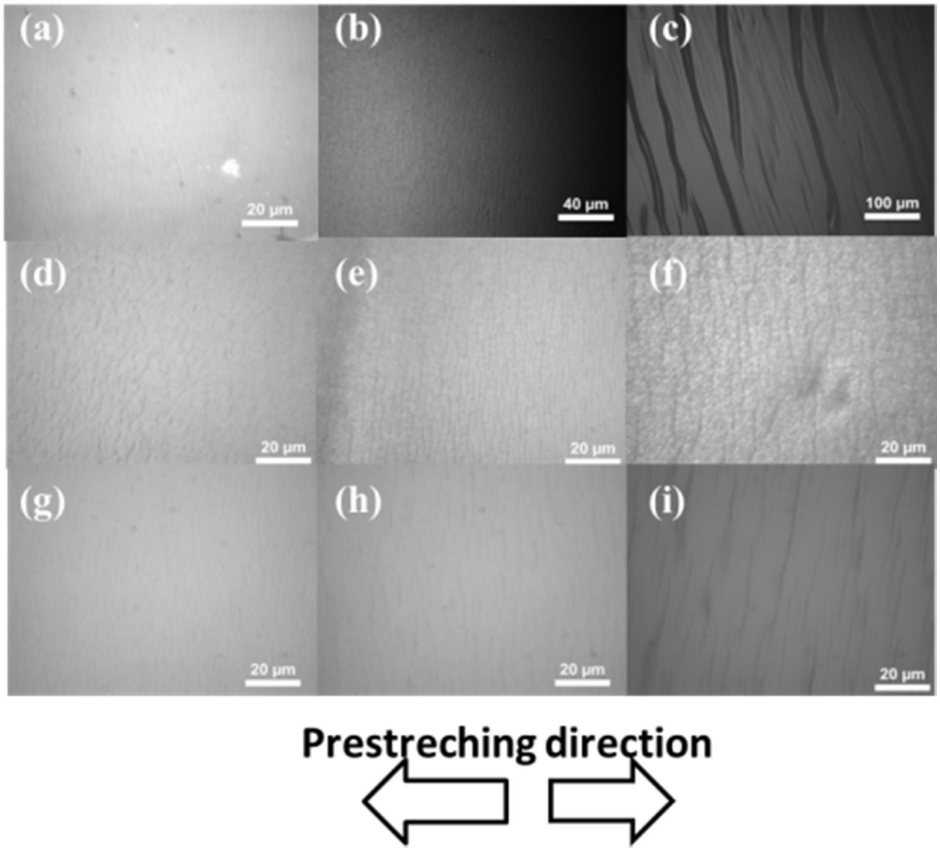

Figure S1. Optical micrographs of 4% pre-strain buckled films of P1 with (a) λ_b=2.07 µm and d_f= 30 nm, (b) λ_b=4.11 µm and d_f= 43 nm, (c) λ_b=38.1 µm and d_f= 410 nm, P2 with (d) λ_b=2.65 µm and d_f= 52 nm,(e) λ_b=3.51 µm and d_f= 90 nm,(f) λ_b=7.54 µm and d_f= 127 nm ,and P3 (g) λ_b=2.11 µm and d_f= 51 nm,(h) λ_b= 3.93 µm and d_f =101nm,(i) λ_b=9.31 µm and d_f= 211 nm.

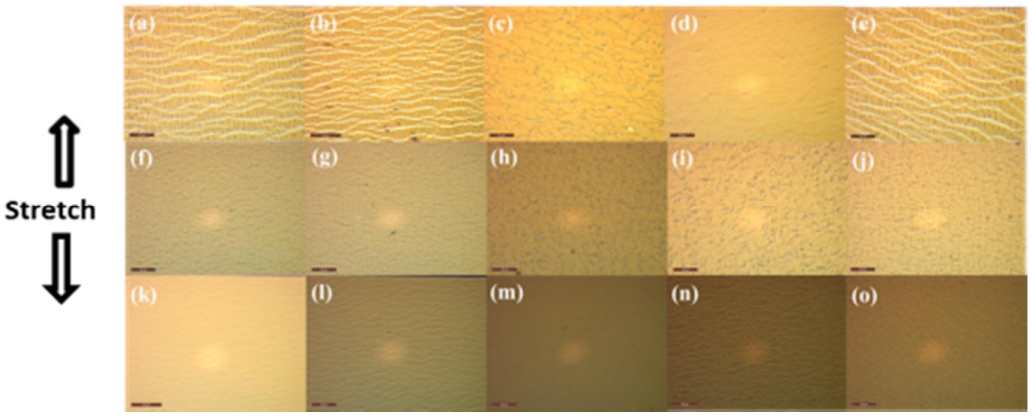

Figure S2. Optical micrographs of thin films of P1 with (a) 80%, (b) 100%, (c) recovered from 50% to 0%, (d) recovered from 100% to 0%, (e) recovered from 100% to 50% strain , P2 with (f) 80%, (g) 100%, (h) recovered from 50% to 0%, (i) recovered from 100% to 0%, (j) recovered from 100% to 50% strain, and P3 with (k) 80%, (l) 100%, (m) recovered from 50% to 0%, (n) recovered from 100% to 0%, (o) recovered from 100% to 50% strain.

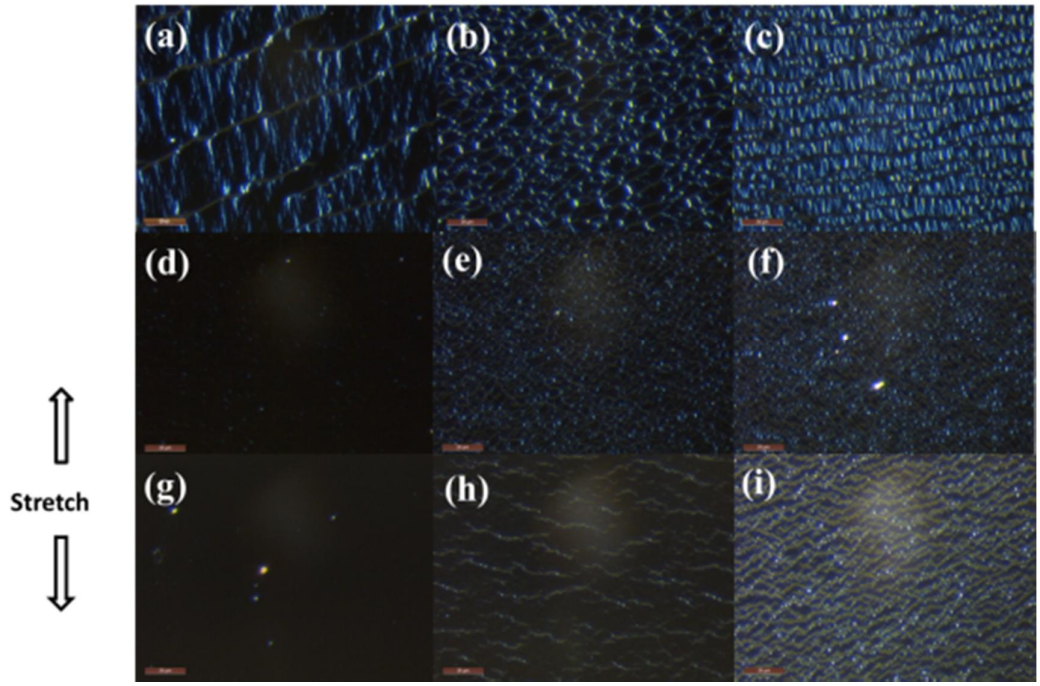

Figure S3. Dark field optical micrographs of thin films of P1 with (a) 10%, (b) 20%, (c) 100% strain, P2 with (d) 10%, (e) 20%, (f) 100% strain ,and P3 with (g) 30%, (h) 50%, (i) 100% strain.

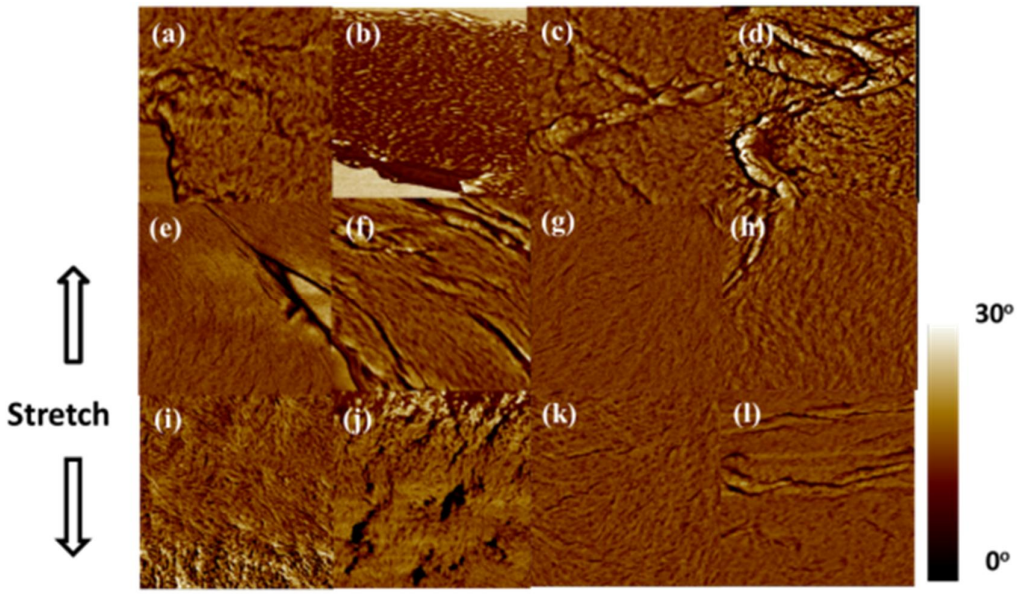

Figure S4. AFM phase images (1μm×1μm) of the polymer thin films: P1 at (a) 80%, (b) 100%, (c) release from 50% and (d) released from 100% strain, P2 at (e) 80%, (f) 100%, (g) release from 50% and (h) released from 100% strain, and P3 (i) 80%, (j) 100%, (k) release from 50% and (l) released from 100% strain.

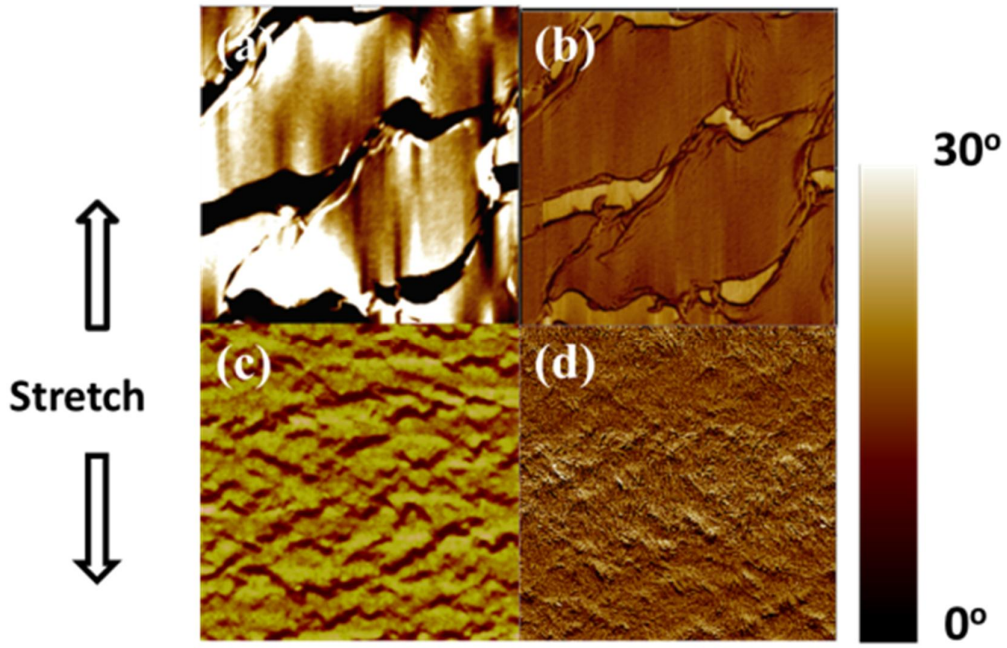

Figure S5. Tapping mode AFM (5μm×5μm) (a) height and (b) phase images of P2, and (c) height and (d) phase images of P3, with 50% applied strain.

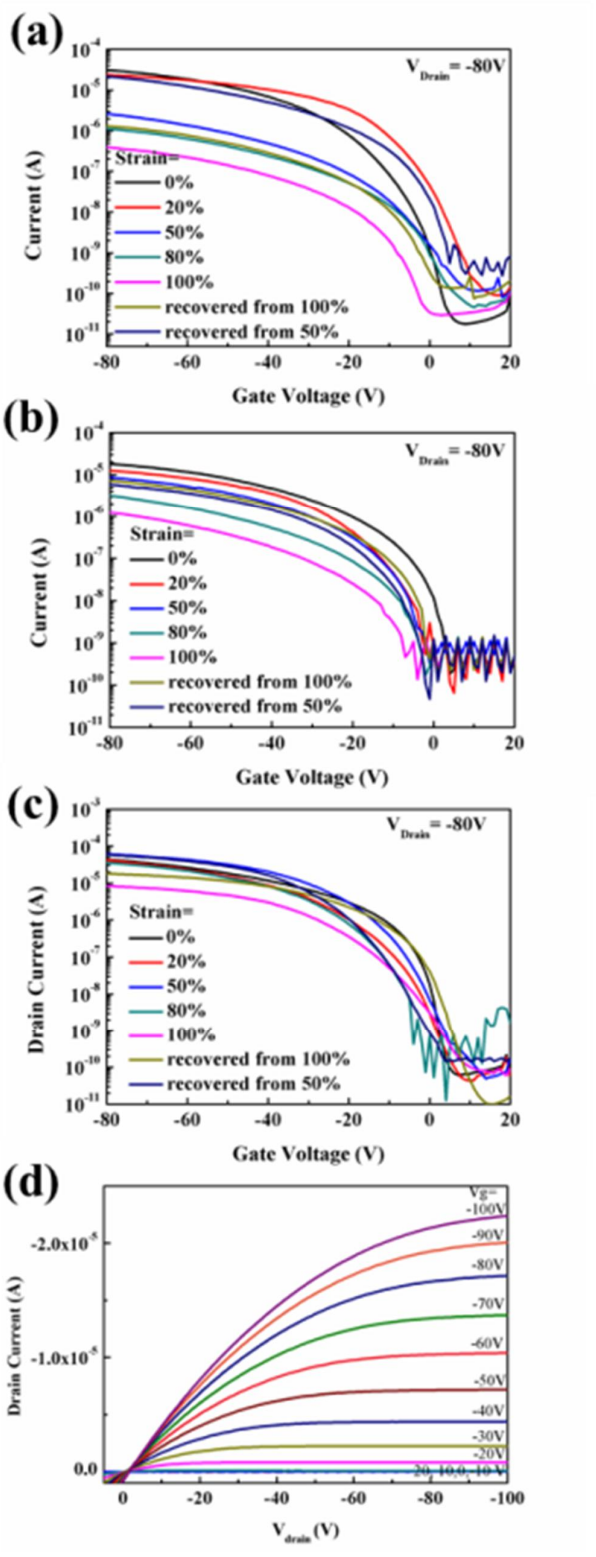

Figure S6. Transfer curves of (a) P1 , (b) P2, and (c) P3 with different applied strain and (d) output curves of P3 with 50% strain

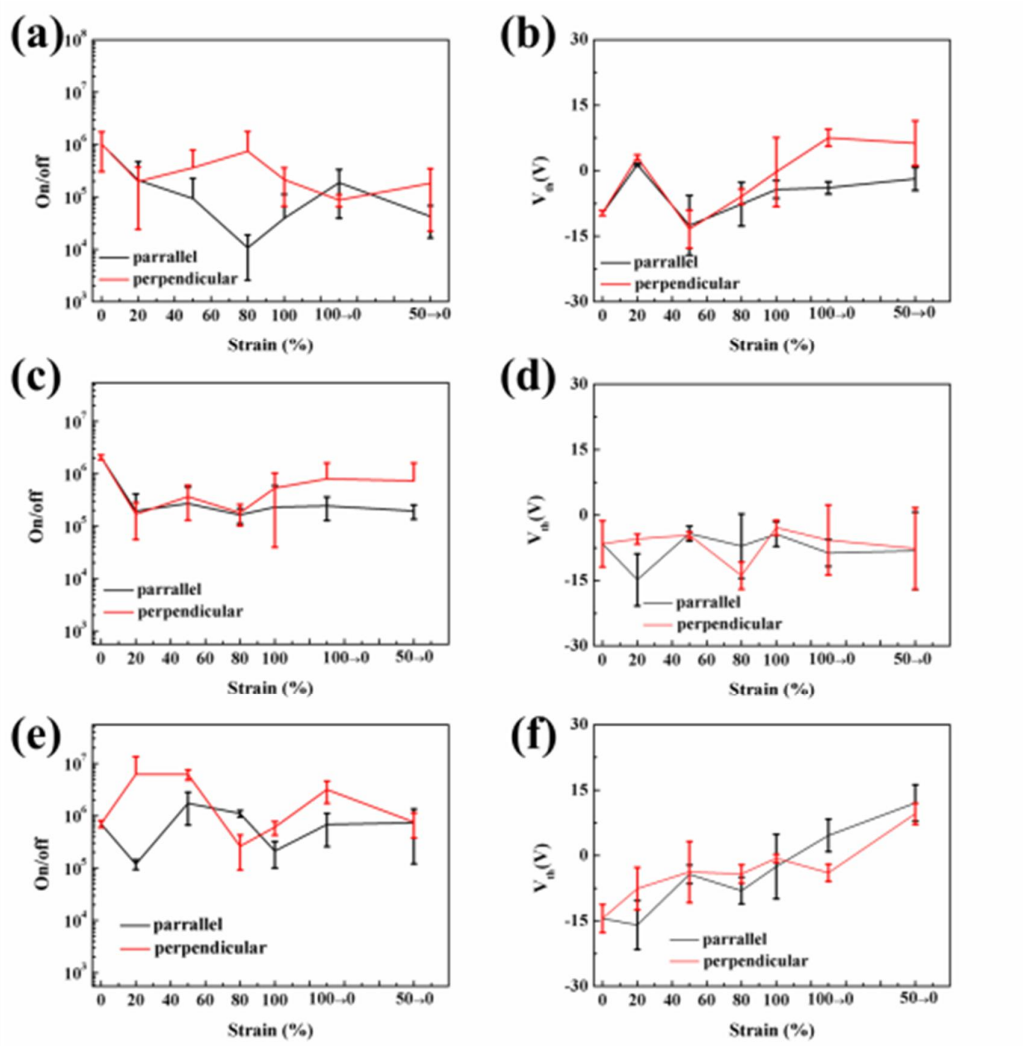

Figure S7. The on/off ratio of (a) P1,(c) P2, (e) P3, and V_{th} of (b) P1,(d) P2, (f) P3 polymer thin films at different strains for transistors with 50 μm channel length.

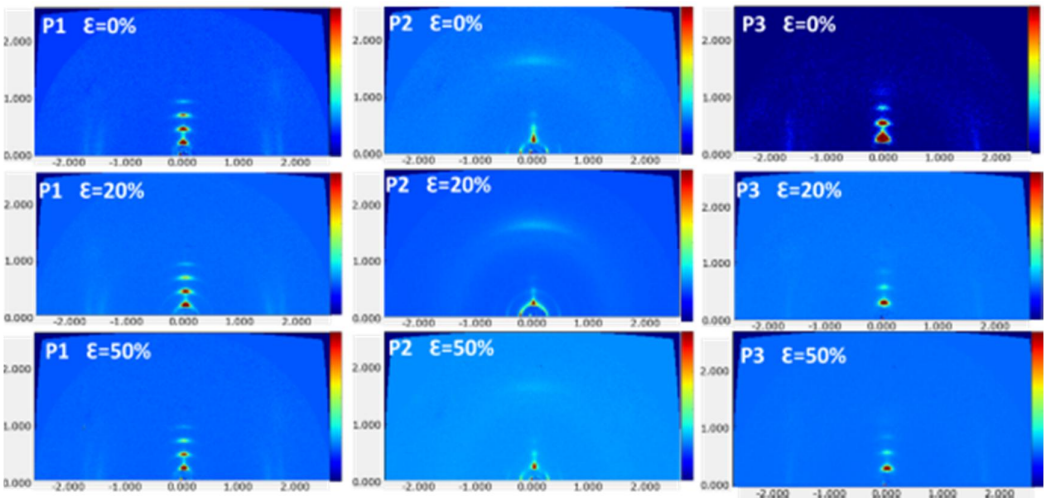

Figure S8. The 2D GIXD diffraction patterns of the transferred polymer films under different strain.

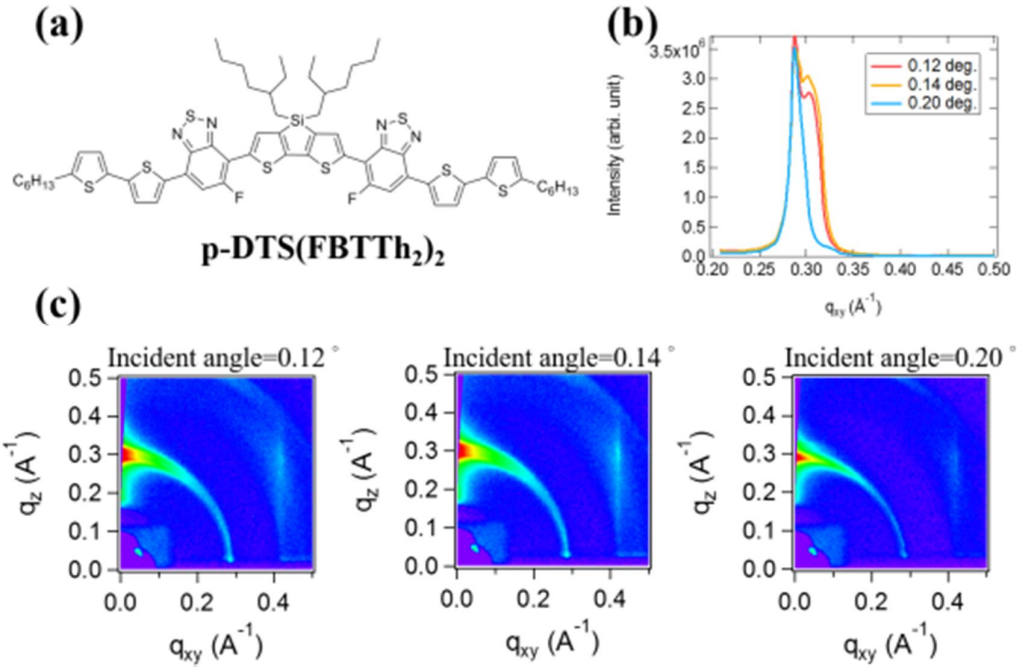

Figure S9. (a) Chemical structure of p-DTS(FBTTh$_2$)$_2$, (b) the out-of-plane 1-D XRD patterns and (c) the GIXD patterns of p-DTS(FBTTh$_2$)$_2$ films with different incident angles.

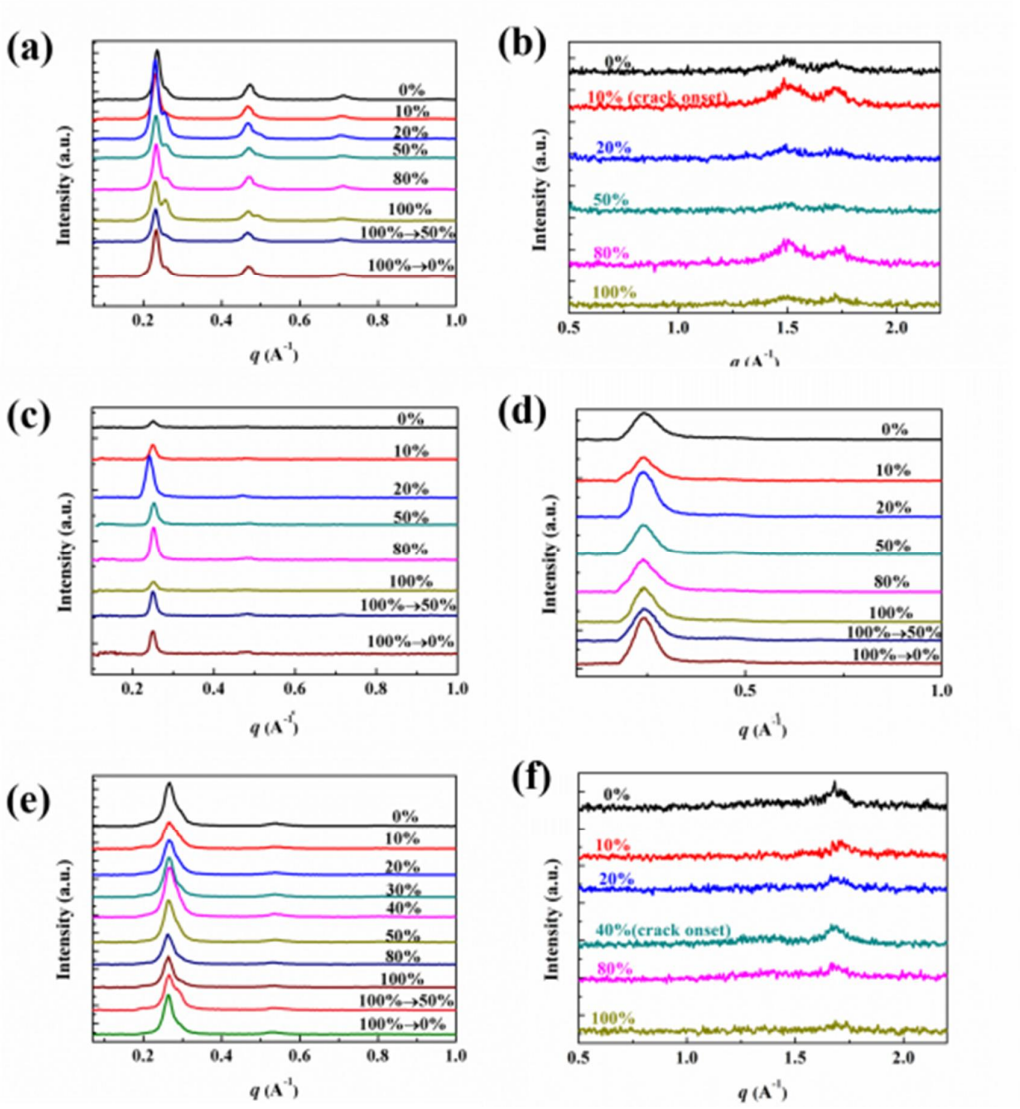

Figure S10. The 1D GIXD profiles of (a) P1 (out-of-plane), (b) P1 (in-plane) (c) P2 (out-of-plane), (d) P2 (in-plane) (e) P3 (out-of-plane) , and (f) P3 (in-plane) at different applied strains, plotted in 2-dimensional axis.

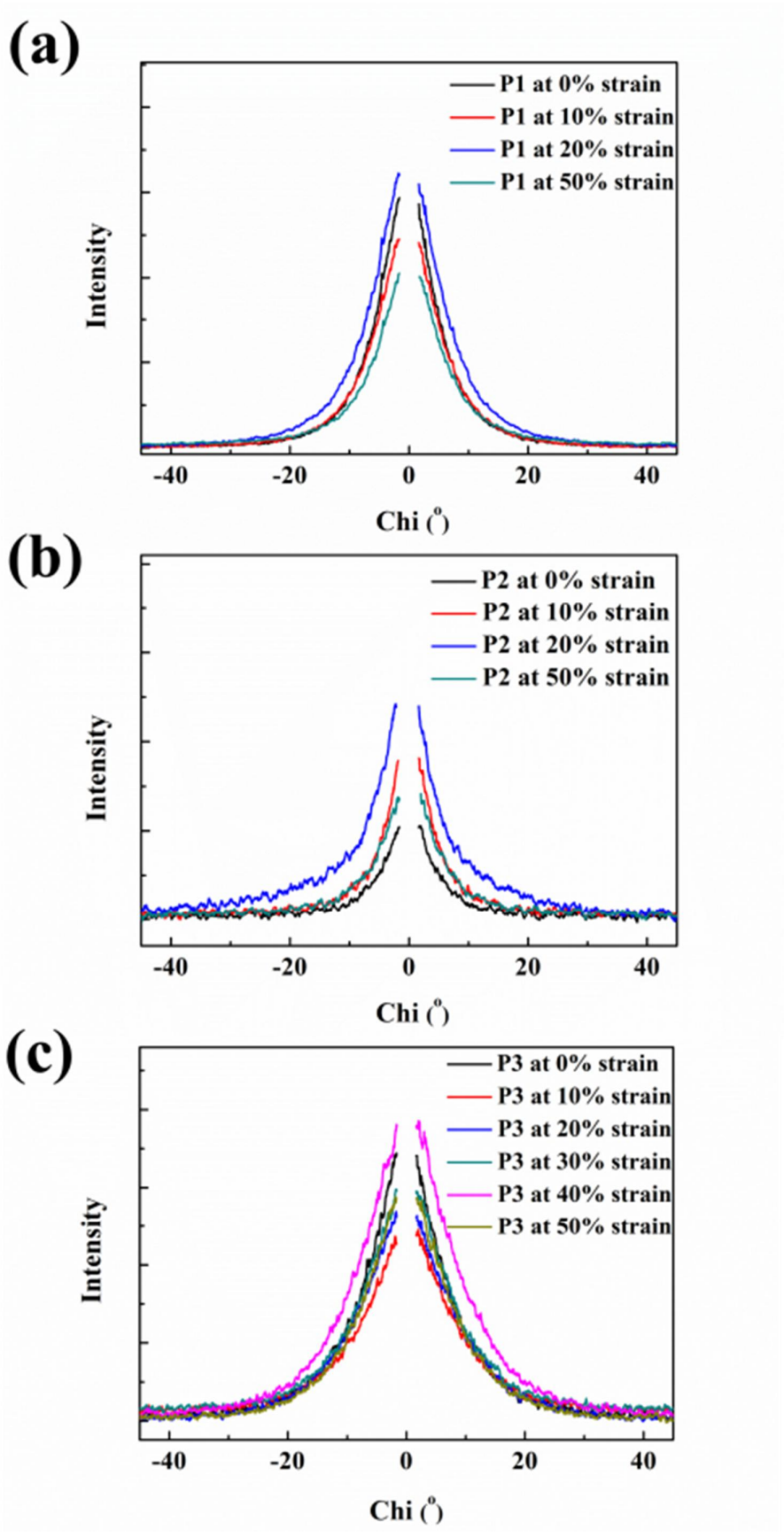
(a)
P1 at 0% strain
P1 at 10% strain
P1 at 20% strain
P1 at 50% strain
Intensity
-40
-20
0
20
40
Chi (°)
(b)
P2 at 0% strain
P2 at 10% strain
P2 at 20% strain
P2 at 50% strain
Intensity
-40
-20
0
20
40
Chi (°)
(c)
P3 at 0% strain
P3 at 10% strain
P3 at 20% strain
P3 at 30% strain
P3 at 40% strain
P3 at 50% strain
Intensity
-40
-20
0
20
40
Chi (°)

Figure S11. The (200) diffraction peaks of the polymers at different strain. Note that the missing data points around chi=0 is due to transforming pole figures into q_{xy}-q_z reciprocal space. Due to the grazing geometry in GIXD experiments, a portion of the reciprocal space near the exact out-of-plane q_z orientation could not be probed.

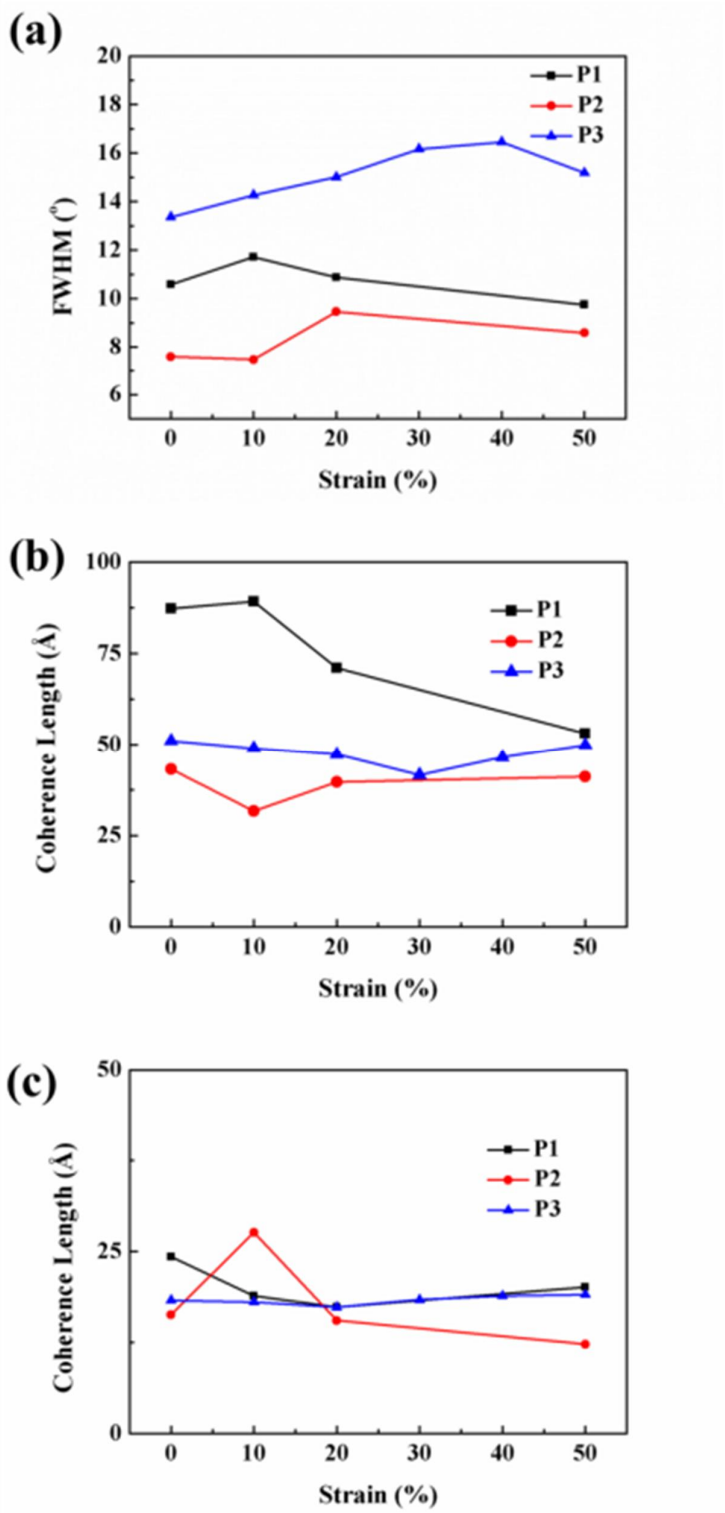

Figure S12. (a) FWHM , (b) L_c of out-of-plane lamellar packing (200) diffractions ,and (c) L_c of π-π stacking of the three studied polymers applied with different strains.

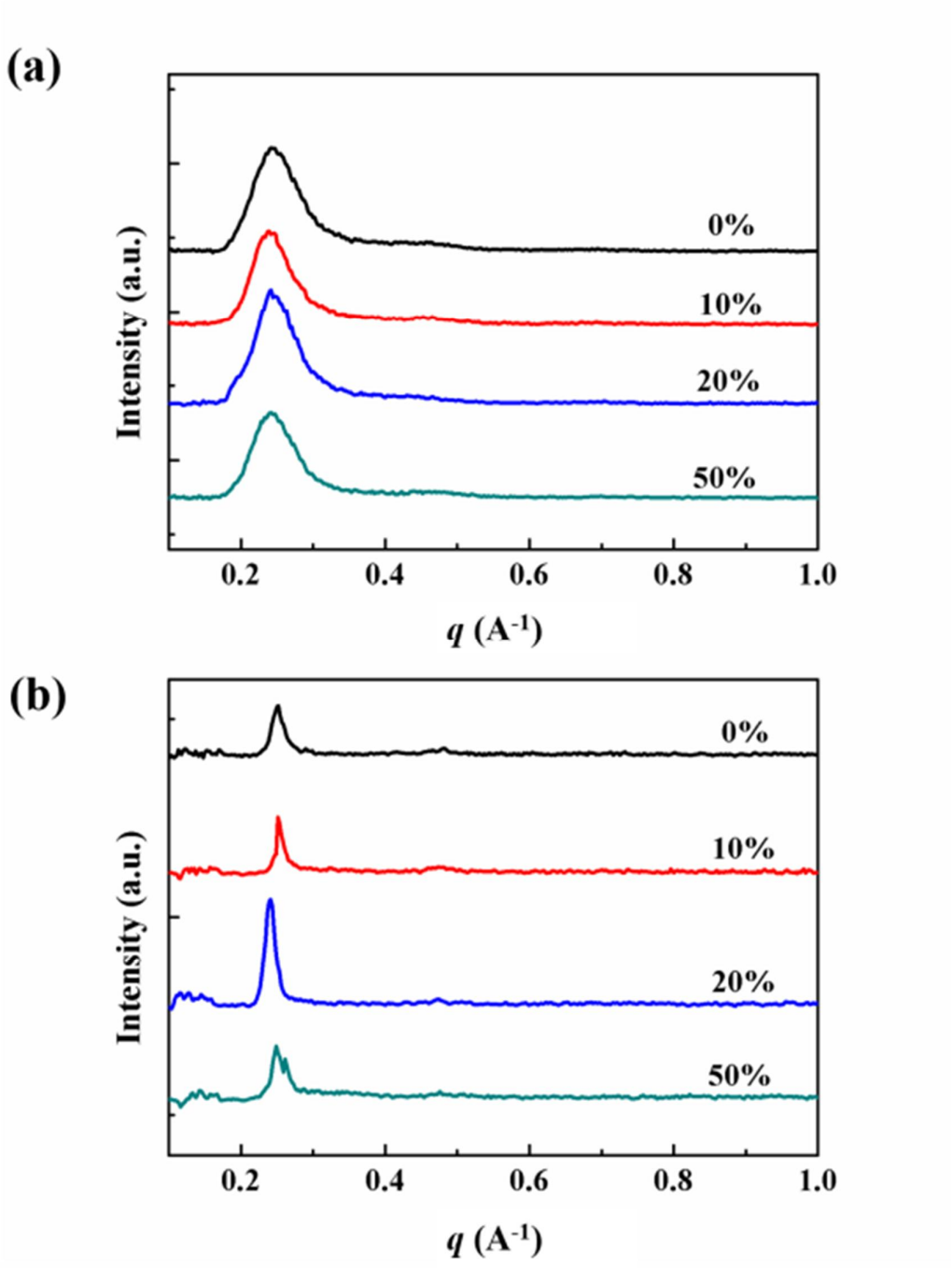

Figure S12. The 1D GIXD profiles of (a) P2 (out-of-plane) and (b) P2 (in-plane) at different applied strains, which X-ray beam is perpendicular to strain direction. Note that the crack onset strains are 10%, 20%, and 40% for P1 ,P2, and P3, respectively.